

**GEDIZ UNIVERSITY ★ GRADUATE SCHOOL OF NATURAL AND
APPLIED SCIENCES**

**METAL-OXIDE NANO STRUCTURES FOR GAS SENSING
APPLICATIONS**

MSc. THESIS

Enis Ekmel TURAL

Nanotechnology Programme

Thesis Supervisor : Asst. Prof. Yavuz BAYAM

November 2014

**GEDIZ UNIVERSITY ★ GRADUATE SCHOOL OF NATURAL AND
APPLIED SCIENCES**

**METAL-OXIDE NANO STRUCTURES FOR GAS SENSING
APPLICATIONS**

MSc. THESIS

**Enis Ekmel TURAL
60071103**

Nanotechnology Programme

Thesis Advisor: Asst. Prof. Yavuz BAYAM

November 2014

GEDİZ ÜNİVERSİTESİ ★ FEN BİLİMLERİ ENSTİTÜSÜ

**GAZ ALGILAMA UYGULAMALARI İÇİN METAL-OKSİT NANO
YAPILAR**

YÜKSEK LİSANS TEZİ

**Enis Ekmel TURAL
60071103**

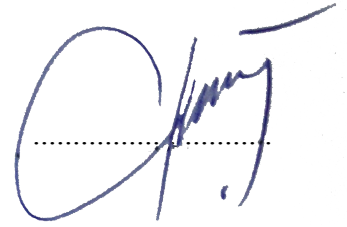
Nanoteknoloji Programı

Tez Danışmanı: Yrd. Doç. Dr. Yavuz BAYAM

Kasım 2014

Enis Ekmel Tural, a **MSc.** student of Gediz University, **Institute of Science with ID No :60071103**, successfully defended the **thesis** entitled “**METAL-OXIDE NANO STRUCTURES FOR GAS SENSING APPLICATIONS**” which, he prepared after fulfilling the requirements specified in the associated legislations, before the jury whose signatures are below.

Thesis Advisor : **Assistant Prof. Yavuz BAYAM**
Gediz University



Jury Members: **Prof.Dr. Mehmet Emin Şengün ÖZSÖZ**
Gediz University



Asst. Prof. Ramazan ATALAY
Gediz University



Asst. Prof. Uğur TÜRKAN
Gediz University



Asst. Prof. Merih PALANDÖKEN
Gediz University



Date of Submission : November 3, 2014

Date of Defense : June 12, 2014

To my parents and future spouse and children,

FOREWORD

I would like to thank my supervisor Asst. Prof. Yavuz BAYAM for his help, advice and support during the master years. His assistance in terms of experimental, theory, and general feedback during the thesis has been crucial for my successful completion. I am very grateful to be working with him.

I would like to thank Prof. Dr. Salih OKUR for letting me work in gas measurement equipments and my precious friend Cebrail Özbek for his help, assistance during the measurements of gas absorptions in the laboratory.

And of course my precious parents, sister, brother, and rest of the family members for their support, love and patience during this thesis. It was very important to have their support.

TABLE OF CONTENTS

ABBREVIATIONS	vii
LIST OF TABLES	viii
LIST OF FIGURES	ix
SUMMARY	xii
ÖZET	xiii
1. INTRODUCTION	1
1.1.Properties at the Nanoscale.....	1
1.2.Indoor Air Quality (IAQ).....	3
1.2.1. Carbon Monoxide	4
1.2.2. Carbon Dioxide (CO ₂)	5
1.2.3. Volatile Organic Compounds (VOCs)	6
1.3.History of Gas Sensing Applications.....	7
2. THEORY	10
2.1.Semiconductors	10
2.2.Metal Oxide Semiconductors	13
2.2.1.Adsorption Mechanism of Metal Oxide Gas Sensors	16
2.3.Zinc Oxide (ZnO)	20
2.3.1.Crystal Structure	21
2.3.2. Gas Sensing Properties of ZnO	22
2.3.3.Growth Techniques For ZnO	23
2.3.3.1.Hydrothermal.....	24
2.3.3.2.Carbothermal Reduction and Solid-State Chemical Reaction	25
2.3.3.3.Molecular-Beam Epitaxy (MBE)	25
2.3.3.4.RF Sputtering.....	26
2.3.3.5.Aerosol Deposition.....	27
2.3.3.6.Thermal Evaporation.....	28
2.3.3.7.Chemical Vapor Deposition (CVD).....	29
2.4.Sonochemistry	32
3. EXPERIMENTAL	35
3.1.Synthesis of ZnO Nanorod for Gas Sensor Application.....	35
3.1.1.Gold(Au) Electrode Deposition.....	35
3.1.2.ZnO Seeding Process.....	38
3.1.3.Growth Process.....	39
3.2.Characterization Techniques.....	43
3.2.1.Optical Microscopy	43
3.2.2.Scanning Electron Microscopy (SEM).....	44
3.2.3.Energy Dispersive X-ray Spectroscopy (EDS).....	46
3.2.4.Raman Spectroscopy	47
4. RESULTS AND DISCUSSION	49
4.1.Morphological Characterization.....	49
4.1.1.Optical Microscopy Analysis.....	49
4.1.2.Scanning Electron Microscopy Analysis.....	54
4.2.Elemental Analysis	59
4.2.1.Energy Dispersive X-ray Spectroscopy (EDS).....	59

4.2.2.Raman Spectroscopy	60
4.3.Gas Absorption Analysis	62
4.3.1.Oxygen (O ₂) Response.....	63
4.3.2.Carbon Monoxide (CO) Response.....	64
4.3.3.Carbon Dioxide (CO ₂) Response	66
4.3.4.Ethanol (C ₂ H ₅ OH) Response.....	68
4.3.5.Isopropyl Alcohol (C ₃ H ₇ OH) Response.....	70
4.3.6.Chloroform (CHCl ₃) Response	73
4.3.7.Dichloromethane (CH ₂ Cl ₂) Response	75
5. CONCLUSION	78
REFERENCES	80
CURRICULUM VITAE.....	88

ABBREVIATIONS

ZnO	: Zinc Oxide
IDE	: Interdigitated Electrode
SEM	: Scanning Electron Microscopy
EDS	: Energy-dispersive X-ray spectroscopy
WHO	: World Health Organization
EPA	: Environmental Protection Agency
IAQ	: Indoor Air Quality
VOC	: Volatile Organic Compounds
1-D	: One Dimensional
MOS	: Metal Oxide Semiconductor
HMT	: Hexamethylenetetramine
IPA	: Isopropyl Alcohol
DCM	: Dichloromethane
PL	: Photoluminescence
QCM	: Quartz Crystal Microbalance
LPG	: Liquefied Petroleum Gas
PAH	: Polycyclic Aromatic Compound
UV	: Ultraviolet
CMOS	: Complementary Metal-Oxide Semiconductor
CCD	: Charge-Coupled Device
IR	: Infrared
RHEED	: Reflection high energy electron diffraction
UHV	: Ultrahigh Vacuum
XRD	: X-ray Diffraction
FTIR	: Fourier Transform Infrared Spectroscopy
CVD	: Chemical Vapor Deposition

LIST OF TABLES

	<u>Page</u>
Table 1.1: Historical landmarks in the development of gas sensors.....	9
Table 2.1: Research papers focusing on nanoscale metal oxide semiconductor gas sensors.....	16
Table 2.2: Resistance change in gas types.....	17
Table 2.3: Basic properties of ZnO.....	21
Table 2.4: Research papers focusing on nanoscale zinc oxide (ZnO) gas sensors.....	31
Table 2.5: Research papers focusing on the sonochemical growth.....	34

LIST OF FIGURES

	<u>Page</u>
Figure 2.1: Electrical conductivity of solids.....	10
Figure 2.2: Energy levels of solids.....	11
Figure 2.3: (a) Fermi function and (b) band diagram for semiconductors.....	12
Figure 2.4: Top 10 metal oxide nanostructured materials used for gas sensor applications in publications since 2002.....	14
Figure 2.5: Schematic diagrams of resistance change of (a) n-type and (b) p-type MOS under reducing gases.....	18
Figure 2.6: Schematic diagram of the depletion layer on the surface of cylinder with a thickness (or width) of L_d , under condition of $D \gg 2L_d$, $D \gg 2L_d$, and $D \sim 2L_d$	19
Figure 2.7: (a) The hexagonal wurtzite structure of ZnO. The O-atoms are the large red spheres and the Zn-atoms are the small blue spheres. (b) Hexagonal faces of wurtzite ZnO nanorod with c-axis [001] orientated growth.....	22
Figure 2.8: Working principle of CVD.....	30
Figure 2.9: Frequency range of sound.....	32
Figure 2.10: The illustration of acoustic cavitation.....	33
Figure 3.1: The image of the thermal evaporator.....	36
Figure 3.2: The image of the mask aligner.....	37
Figure 3.3: The illustrated figure of gold electrodes on the glass substrate....	38
Figure 3.4: The illustrated figure of seed layer on the glass substrate.....	39
Figure 3.5: The image of the ultrasonic processor set up.....	40
Figure 3.6: Structure of hexamethylenetetramine (HMT); blue spheres are nitrogen (N), black spheres are carbon (C) and white spheres are hydrogen (H) atoms.....	41
Figure 3.7: The illustrated figure of ZnO nanorod grown on IDE.....	41
Figure 3.8: The illustrated figure of ZnO nanorod growth process, on the glass substrate.....	42
Figure 3.9: The image of ZnO growth mixture solution; (a) before sonication, (b) after sonication.....	42
Figure 3.10: Optical microscopy system used for the thesis.....	44
Figure 3.11: (a) Schematic working presentation of a SEM instrument, (b)The SEM instrument used for the characterization of ZnO nanorods.....	45

Figure 3.12: Working principle of EDS.....	46
Figure 3.13: Energy level diagram of exciting states in the Raman effect.....	48
Figure 4.1: The image of IDE; (a) before the deposition ZnO nanorods, (b) after the deposition ZnO nanorods.....	50
Figure 4.2: Optical image of ZnO seed layer taken from 4 different areas; (a) and (b) areas are under low magnification (50x), (c) and (d) areas are under high magnification (100x).....	51
Figure 4.3: Optical image of ZnO nanorod taken from 4 different areas; (a) and (b) areas are under low magnification (50x), (c) and (d) areas are under high magnification (100x).....	52
Figure 4.4: Optical image of ZnO nanorod without seed layer of a trial sample taken from 4 different areas; (a) and (b) areas are under low magnification (50x), (c) and (d) areas are under high magnification (100x).....	53
Figure 4.5: SEM images of ZnO seed layer; (a) and (b) are low magnifications (10000x-20000x respectively), (c) and (d) are high magnifications (50000x-100000x respectively).....	55
Figure 4.6: SEM images of ZnO nanorods; (a) and (b) are low magnifications (5000x-10000x respectively), (c) and (d) are high magnifications (20000x-40000x respectively).....	56
Figure 4.7: SEM images of ZnO nanorod on IDE electrodes; (a) and (b) are low magnifications (2500x-5000x respectively), (c) and (d) are high magnifications (10 000x-20 000x respectively).....	57
Figure 4.8: EDS spectrum of ZnO nanorod gas sensor.....	59
Figure 4.9: SEM image of EDS spectrum.....	60
Figure 4.10: Raman spectrum of ZnO nanorod grown on glass substrate.....	61
Figure 4.11: Schematic diagram of gas measurement system.....	62
Figure 4.12: The Resistance (R) - Time (T) measurement of ZnO nanorod gas sensor under O ₂	64
Figure 4.13: The Resistance (R) - Time (T) measurement of ZnO nanorod gas sensor under CO.....	65
Figure 4.14: The Resistance (R) - Time (T) measurement of ZnO nanorod gas sensor under CO ₂	67
Figure 4.15: Routes of oxidation of ethanol vapor.....	68
Figure 4.16: The Resistance (R) - Time (T) measurement of ZnO nanorod gas sensor under ethanol.....	69

Figure 4.17: Linear measurement of ZnO nanorod gas sensor under ethanol.....	70
Figure 4.18: The Resistance (R) - Time (T) measurement of ZnO nanorod gas sensor under IPA.....	71
Figure 4.19: Linear measurement of ZnO nanorod gas sensor under IPA.....	72
Figure 4.20: The Resistance (R) - Time (T) measurement of ZnO nanorod gas sensor under chloroform.....	73
Figure 4.21: Linear measurement of ZnO nanorod gas sensor under chloroform.....	74
Figure 4.22: The Resistance (R) - Time (T) measurement of ZnO nanorod gas sensor under DCM.....	75
Figure 4.23: Linear measurement of ZnO nanorod gas sensor under DCM.....	76
Figure 4.24: Sensitivity values of ZnO nanorod gas sensor for used target gases.....	77

METAL-OXIDE NANO STRUCTURES FOR GAS SENSING APPLICATIONS

SUMMARY

In this MSc. Thesis, direct growth of Zinc Oxide (ZnO) nanorod and their implementation as gas sensor applications are reported. ZnO nanorod gas sensor application mainly involves detection of oxygen (O_2), carbon monoxide (CO), carbon dioxide (CO_2), ethanol (C_2H_5OH), isopropanol (C_3H_7OH), chloroform ($CHCl_3$) and dichloromethane (CH_2Cl_2) gases. The ZnO nanorod sensor essentially contains an Au interdigitated electrode (IDE) structure, which is deposited by conventional photolithography on a microscope glass. The nanorods are grown by using sonochemical growth technique at room ambient. The main purpose of ZnO sensor development is to detect the physical signals and evaluate changes in electrical resistance under target gases. When the n-type metal oxide sensor is under oxygen ambient, it adsorbs O_2 molecules. These molecules receive electrons from the conduction band of the metal oxide and produce O^- , O^{2-} ions, this process results increase the resistance of the sensor. Then, when this sensor is under reducing gases, these gases react with the produced O^- , O^{2-} ions donate electrons to the conduction band of metal oxides. Therefore, the resistance of the sensor decreases. The optical, structural and electrical properties of the device were examined by Scanning Electron Microscopy (SEM), Energy-dispersive X-ray spectroscopy (EDS), Raman Spectroscopy and Gas Absorption Measurement System. Gas absorption measurement has been done in a closed chamber. SEM and EDS results indicate that the glass substrate is fully covered with ZnO nanorods. The resistivity and sensitivity measurements of sonochemically grown ZnO nanorod gas sensor for gas sensing applications suggest that sonochemical growth technique can be a very good alternative for growth one dimensional (1-D) ZnO nanostructures for sensor applications.

GAZ ALGILAMA UYGULAMALARI İÇİN METAL-OKSİT NANO YAPILAR

ÖZET

Bu yüksek lisans tezinde, doğrudan üretilmiş çinko oksit (ZnO) nanoçubuk tabanlı aygıt ve bir gaz sensör uygulaması olarak uyarlanması bildirilmiştir. ZnO nanoçubuk gaz sensör uygulaması oksijen (O₂), karbon monoksit (CO), karbon dioksit (CO₂), etanol (C₂H₅OH), izopropanol (C₃H₇OH), kloroform (CHCl₃) ve diklorometan (CH₂Cl₂) gazlarını içerir. Bu ZnO nanoçubuk tabanlı sensör aslında cam üzerinde klasik fotolitografi yöntemiyle hazırlanmış altın elektrot yapılarını içerir. Nanoçubuklar sonokimyasal büyütme tekniği ile oda sıcaklığında büyütülmüşlerdir. Geliştirilen ZnO sensörün asıl amacı hedef gazlar altında fiziksel sinyalleri belirlemek ve değişimlerin elektriksel dirençlerine olan etkisini incelemektir. N-tip metal oksit sensör oksijen ortamında olduğunda ortamdaki O₂ moleküllerini adsorbe eder. Bu moleküller iletim bandındaki elektronları alarak O⁻, O²⁻ iyonlarını oluşturur. Bu işlemin sonucu olarak sensörün direnci artmış olur. Daha sonra sensör indirgen gazlar altında olduğunda, meydana gelen O⁻, O²⁻ iyonlarıyla reaksiyona girip iletim bandına elektron verir. Böylece, sensörün direnci düşmüş olur. Cihazın optik yapısal ve elektriksel özellikleri Taramalı Elektron Mikroskobu (SEM), Enerji dağılımlı X-ışını spektroskopisi (EDS), Raman Spektroskopisi ve Gaz Soğurma Ölçüm Sistemi yardımıyla incelenmiştir. Gaz soğurma ölçümü kapalı bir haznede yapılmıştır. SEM ve EDS sonuçları cam yüzeyin ZnO nanoçubuklar ile tamamen kaplı olduğunu göstermektedir. Gaz algılama uygulamalarında sonokimyasal yolla büyütülmüş ZnO nanoçubuk gaz sensörün direnç ve hassasiyet ölçümleri göstermektedir ki sonokimyasal büyütme tekniği sensör uygulamalarında bir boyutlu (1-D) ZnO nanoyapıları büyütme için çok iyi bir alternatiftir.

1. INTRODUCTION

All the research and development has been designed to improve the quality of life. It is important to live in an environment which has good air quality. Accordingly, scientists are working intensively on the designing gas detectors to sense the toxic gases and control of these emissions. In the following sections, information about the indoor air quality, sources and effects on health of toxic gases will be explained. The principle of gas sensors is the change of the physical (conductivity, volume and vibration) properties of sensing materials by the adsorption of the target gas on the sensing surface. Increasing sensitivity of gas sensors depends on the increase of surface temperature of the sensing material. Gas sensors need to work on the room temperature for indoor air quality. Hence, we need to increase the surface of sensing material since increasing the indoor temperature is not possible.

In this thesis, zinc oxide (ZnO) nanorods, which have high surface area and aspect ratio, have been produced sonochemically and surface morphology material and sensing properties were investigated.

1.1. Properties at the Nanoscale

Nanotechnology is a science, which deals with the matter at the nanoscale, at the dimensions between 1–100 nm, where unique features enable novel applications. Nanoscience encloses imaging, measuring, modeling, and manipulating matter at the nanoscale. The Properties of the materials are indicated by size in nano scale range. Thus, when the particle size is rooted to the nanoscale, properties such as melting point, fluorescence, electrical conductivity, magnetic permeability, and chemical reactivity change as a function of the size of particle.

Nanostructures exhibit different physical and chemical properties compared to bulk structure. The properties of materials do not depend on composition and structure in the usual sense of that material at nanoscale. Nanomaterials display new phenomena based on the quantized effects. Quantized effects arise in the nanometer regime since the overall dimensions of objects are comparable to the characteristic properties for fundamental excitations in materials [1].

Nanosized materials have very large surface areas compared to the similar masses of bulk materials. If the surface-mass ratio increases, the high amount of the material can be contacted with surrounding materials, thus affecting its reactivity.

Some nanostructured materials like Fe, Co, Ni, Fe₃O₄, etc., are stronger or have different magnetic properties compared to other forms or sizes of the same material. For semiconductors such as ZnO, CdS, and Si the band gap changes with size. Thus, these materials conduct heat or electricity to a greater degree than the bulk forms. They may become more chemically reactive or reflect light better or change color as their size or structure is altered [2]. For example, if we compare the optical properties of ZnO, bulk ZnO particles block UV light, scatter visible light, and appear white whereas, nanosized ZnO blocks UV light, doesn't scatter visible light, because the wavelength of nanosized ZnO is so small compared to the wavelength of visible light and appears transparent. Melting point of ZnO is also altered at the nanoscale.

There are many environmental applications in nanotechnology. For instance, treatment of the wastewater in both bulk-scale and portable applications is facilitated by the help of nanoparticles.

1.2. Indoor Air Quality (IAQ)

World Health Organization (WHO) defines air pollution as, “Air pollution is contamination of the indoor or outdoor environment by any chemical, physical, or biological agent which modifies the natural characteristics of the atmosphere”. There are a lot of sources of air pollution. Generally, these sources can be given as household combustion devices, motor vehicles, industrial facilities, and forest fires. However, there are many different specific sources [3].

Indoor air quality (IAQ) is known as a significant environmental and health problem in many countries. In last several years, scientific researches indicated that the indoor air has more pollution than the outdoor air in industrialized cities. On the other hand, regulated reports indicated that people spend approximately 90% of their time indoors, such as, school and workplace, according to estimates done by Environment Protection Agency (EPA). Therefore, maintaining indoor air quality in schools and the workplace is becoming a top priority.

There are many indoor air pollutants, such as, toxic gases (carbon monoxide (CO), carbon dioxide (CO₂), ozone (O₃), oil, kerosene, polycyclic aromatic compounds (PAHs), coal, dust on floors, and smoke. These pollutants may be released from many sources. Every product which we use in the buildings, can release pollutants to the indoor environment such as; tobacco products, products for household cleaning and maintenance, asbestos-containing insulations, building and furnishing materials, wet or damp carpet, personal care or hobbies, central heating and cooling systems and pollutants, which come from outdoor sources such as radon and pesticides [4].

The risks on healths, for many people, can be higher due to exposure to air pollution indoors than outdoors. People can react differently to different levels of substances according to the age, quantity and pollutant. People who are exposed to indoor air pollutants for the long period of time may have chronic illnesses, especially respiratory and cardiovascular diseases. In the lower period of exposures, there are many symptoms caused by air quality according to an individual's sensitivity. These symptoms are chills, sweating, eye irritation, allergies, coughing, sneezing, nausea, fatigue, skin irritation, breathing difficulty, blacking out and many others [5].

In the previous paragraph, the primary cause of indoor air-quality problems in houses was mentioned. If the people do not take precautions, the amount of pollutants will keep increasing. Therefore, ventilation system is primary necessity for closed environments, and it shouldn't be inadequate. The outdoor air should be coming to the indoor environment to carry the pollutants to the outside. It is also possible that high temperature and humidity levels can increase the concentration of the pollutants.

As it was mentioned before, there are many gases that we face off within indoor environment. Many of them cause death or chronic diseases. In this thesis, many indoor air pollutants which are carbon monoxide (CO), carbon dioxide (CO₂), and volatile organic compounds (VOCs) were measured.

1.2.1. Carbon Monoxide

Carbon monoxide (CO) is a most common odorless, colorless, and toxic gas that we face in the closed environments. It's impossible to see, taste, or smell the toxic fumes and interferes with the delivery of oxygen throughout the body. CO can kill you before you are aware of its

presence. The health problems of CO at lower concentration might show similar symptoms like the flu because symptoms are headaches, dizziness, disorientation, nausea, and fatigue. EPA specifies average levels of CO to 0.5 to 5 parts per million (ppm) in houses without gas stoves. The levels on properly adjusted gas stoves are often 5 to 15 ppm and on poorly adjusted stoves may be 30 ppm or higher. Therefore, a detector should be applied in the houses [6].

Combustion systems, i.e., heaters burned by fuel oil or solid oil and fire places, and automobile exhausts are the common sources of CO. Incomplete oxidation during combustion may cause high concentrations of carbon monoxide in the indoor air, or if the flue is improperly sized, blocked, disconnected, or is leaking. Smoking at home is also another source of CO.

It's important to reduce the exposure of carbon monoxide in the indoors. Some precautions must be taken in the buildings. Natural gas heating systems need to be applied. Ventilation system should be carefully built into the buildings. Additional ventilation can be used as a temporary measure when high levels of CO are expected for short periods of time. Gas appliances need to be kept properly adjusted. Proper fuels need to be used in kerosene space heaters. Exhaust fan should be vented to outdoors over gas stoves. Flues need to open when fireplaces are in use [7].

1.2.2. Carbon Dioxide (CO₂)

Carbon dioxide (CO₂) gas is one of the natural components in the atmosphere as part of the Earth's carbon (C) cycle (the natural circulation of C among the atmosphere, oceans, soil, plants, animals and micro-organisms). Human activities are increasing the amount of CO₂ by emitting greenhouse gas, combustion of fossil fuels (coal, natural gas,

and oil) for energy and transportation, although certain industrial processes and land-uses change and emit CO₂. Human activities also have effect on natural sinks, forests, to remove CO₂ from the atmosphere [6].

The outdoor air contains 350 - 400 ppm concentration of carbon dioxide in urban locations. There is higher concentrations of CO₂ in the cities which have high vehicle traffic and combustion areas, industrialized. Carbon dioxide concentrations in the indoors can vary from 100 ppm to over 1000 ppm according to the time and outdoor air ventilation.

The levels of CO₂ in the closed environments change according to the number of people in that room, how long that area has been kept closed, the amount of fresh air and size of the room or area.

At high levels, CO₂ has also negative effects on health such as headache, dizziness, nausea, fatigue, eye symptoms, nasal symptoms, respiratory tract symptoms, and total symptom scores. This could occur when someone exposed to CO₂ above 5,000 ppm for many hours.

1.2.3. Volatile Organic Compounds (VOCs)

Volatile organic compounds (VOCs) are in everywhere, both in the indoor and outdoor environments. They are emitted as gases from certain solids and liquids. VOCs include a lot of chemicals, and they have a very low vapor pressure, so they evaporate directly into the air. Some of them may cause short-term and long-term adverse health effects. Concentrations of many VOCs are ten times higher in the indoors than outdoors.

A lot of materials and products contain VOCs. In the indoors, paints, lacquers, paint strippers, cleaning, disinfecting, cosmetic, degreasing supplies, pesticides, building materials and furnishings in

houses; in the offices, equipments such as copiers and printers, correction fluids and carbonless copy paper, graphics and craft materials, including glues and adhesives, permanent markers, and photographic solutions emit VOCs. All of these products may release organic compounds while you are using them.

The negative effects on health that VOCs caused are like the other indoor air contaminants. Eye, nose, and throat irritation; headaches, loss of coordination, nausea; damaging liver, kidney, and central nervous system are some of the health effects that VOCs caused. Some of VOCs are suspected or known to cause cancer in humans. Exposing VOCs have many symptoms, which are conjunctival irritation, nose and throat discomfort, headache, allergic skin reaction, dyspnea, declines in serum cholinesterase levels, nausea, emesis, epistaxis, fatigue and dizziness [7].

1.3. History of Gas Sensing Applications

The first gas detector was placed in the market in 1923. It was covered with hot platinum wire to ensure working at several hundred degrees, detecting combustible gases in an atmosphere. The operating process simply depends on measuring the resistance change resulting from the temperature.

In 1960s, the world needed for better gas sensors to prevent the accidental explosion of gas involving liquefied petroleum gas (LPG). LPG was using for heating and cooking at homes. Therefore, researchers focused on lower cost and more sensitive gas sensors. World's first semiconductor gas sensor was reported by Seiyama, T. [8] in 1962. They utilized the metal-oxide semiconductor (zinc oxide) mechanism, that based on the measurement of resistance change upon gas adsorption. This system led the researchers to development of the metal-oxide based gas sensor. Taguchi, N. invented a tin oxide (SnO_2) gas sensor and

patented it at the same time [9]. This invention and the research on inflammable, explosive and toxic gases played a role on decreasing the gas accidents and also triggered investigations into gas sensors for occupational safety.

Matsusita Electric Industrial Corp.® developed humidity sensor and placed sensor in the electronic oven for automated cooking. This sensor measured alteration in humidity at increasing temperature and was made of porous composites of metal oxides.

After the 1980s the gas sensing technologies had been placed in the market as a gas detector product for inflammable or explosive gases, toxic gases, oxygen, and humidity [10].

The historical landmarks of gas sensor development are given in Table 1.1 chronologically. It contains very important gas sensing applications from 1904 to 2008 in the world. First oxygen sensor, first semiconductor gas sensor, first electronic nose and many landmarks are shown in the table. Kautsky's first oxygen sensor uses the phosphorescence quenching dyes. These dyes change luminescence linearly and reversibly by single-photon to sense O₂ molecules [11]. Persaud designed the first electronic nose by using semiconductor transducers, and this device can be reproducibly discriminate between a wide range of odors [12].

At present, gas sensors are developing according to the nanotechnology for the large surface area and high sensitivity, and nanotechnology presents many methods on many different materials. Gas sensors are playing an important role in our lives. They used for environmental analysis, indoor air quality, occupational safety, public security and food quality control. All of these factors are linked to human health.

Table 1.1 Historical landmarks in the development of gas sensors [13].

Year	Developer	Event
1904	Kohlrash F. and Nernst W.	Thermal Conductivity-based gas sensor
1931	Kautsky H. and Hirsch A.	First Oxygen Sensor
1953	Brattain W. and Bardeen J.	Gas Adsorption influence on semiconductor conductance
1959	Baker A.	Catalytic bead gas sensor (pellistor)
1962	Seiyama T. and Taguchi N.	Semiconductor (ZnO) gas sensor
1963	Goto K. and St. Pierre G.R.	Solid electrolyte gas sensor
1964	King W.H. Jr.	Coated piezoelectric quartz crystals as sensors for water, hydrocarbons, polar molecules, and hydrogen sulfide
1970	Taguchi N.	SnO ₂ based gas sensor
1974	Chiang C.K. et al.	First polymer based conductometric gas sensor
1975	Lundstrom I. et al.	Gas-FET
1979	Wohltjen H. and Dessey R.	Surface acoustic wave(SAW) sensors for gases
1982	Persaud K.C. and Dodd G.	Electronic Nose
1984	Hall, J.P. et al.	Thermoelectric (Pyroelectric Effect) gas sensors
1985	Mc Aleer J.F. et al.	Thermoelectric (Seebeck Effect) gas sensors
1993	Abraham M.H. et al.	Fullerenes app. in gas sensors
1996	Dresselhaus M.S. et al.	Carbon nanotubes in sensor app.
2002	Comini E. et al.	1-D Metal-oxide based conductometric gas sensor
2008	Javey A. et al.	First integrated nanowire sensor circuit

2. THEORY

2.1. Semiconductors

All solids can be classified as conductors, semiconductors, or insulators according to the availability of conduction electrons in their structures. As a class of materials, semiconductors played a pivotal role in the growth of our scientific and technological development over the last six decades.

Solids are classified into two categories due to their electrical conductivity. Figure 2.1 represents distinction between insulators and conductor as an electrical conductivity. Materials which have physical features between these two categories are called as semiconductors.

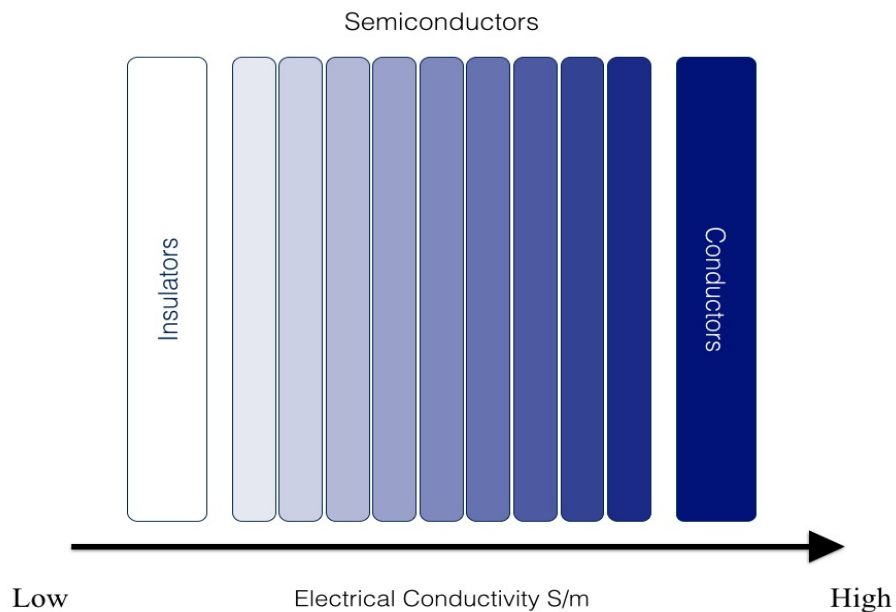


Figure 2.1 Electrical conductivity of solids.

A semiconductor is a substance which cannot conduct electricity at the room temperature but at higher temperatures, it can conduct electricity. The conductivity of semiconductors depends on external conditions. Additionally, conductivity of these materials is predetermined inherently according to interatomic bonds [14]. Two most

commonly used semiconductors are Germanium (Ge) and silicon (Si). The crystalline structures of semiconductors are formed by covalent bonds.

The electrons in the outermost orbit of an atom are called as valence electrons and the range of energy, which possesses these electrons is valence band. The band of energy which can free electrons from binding its own atom to move randomly within the atomic lattice is called conduction band.

The separation between conduction band and valence band on the energy level diagram is known as forbidden energy gap. In this energy gap, no electron of a solid can stay and there is no allowed energy state in this region. The forbidden energy gap is different in insulators, conductors and semi conductors. Figure 2.2 shows these differences and energy levels of solids.

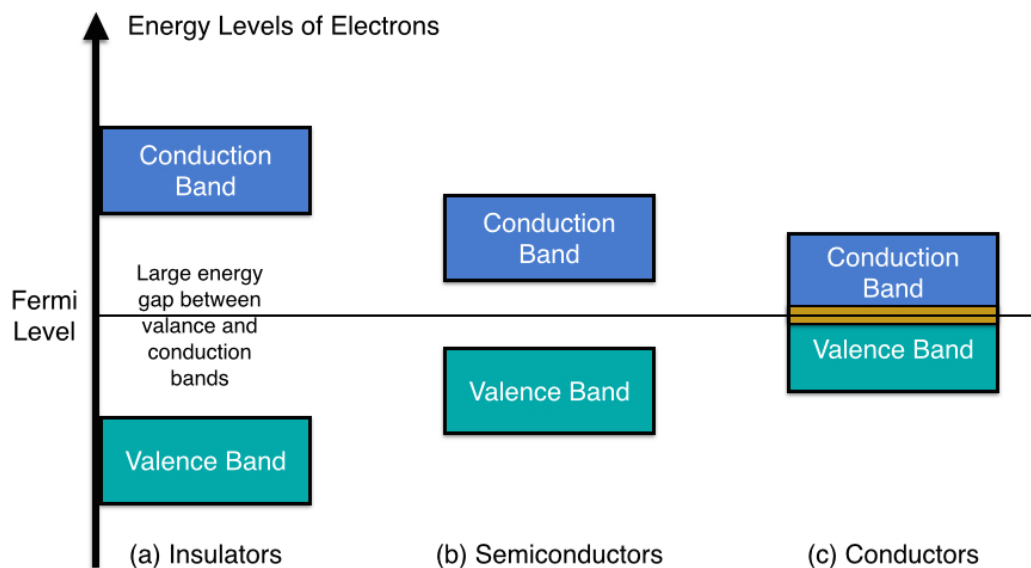


Figure 2.2 Energy levels of solids.

The Fermi level is the highest occupied state at $T=0$. Semiconductors have a large energy band gap from 0.5 to 5.0 eV. There

is no conduction occurs at the energies below Fermi level. The illustrated Fermi level band diagram of semiconductors is shown in Fig. 2.3 [15].

In the figure, electron energy levels are represented on the y-axis and the distance through the crystal is represented on the x-axis. When electrons begin to occupy the conduction band above Fermi Level, conductivity increases [16].

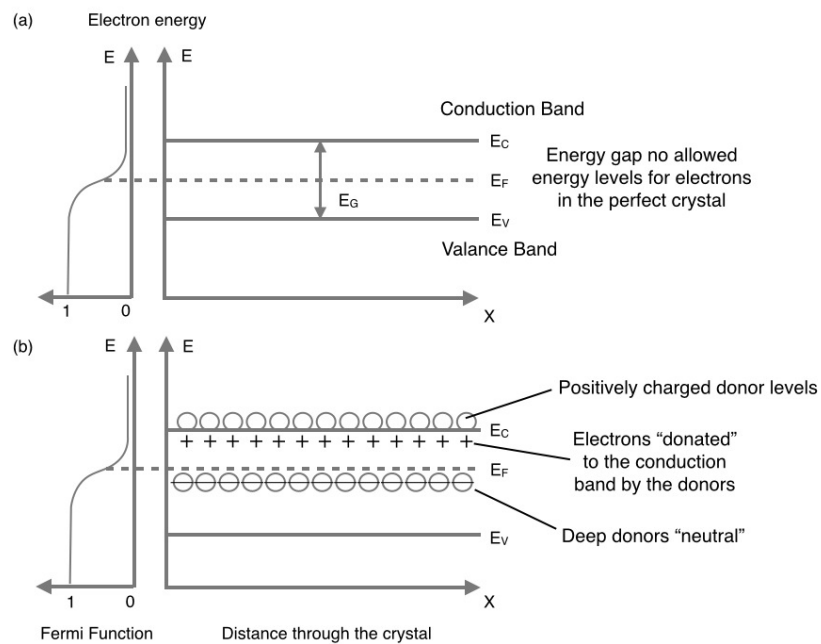


Figure 2.3 (a) Fermi function and (b) band diagram for semiconductors.

Semiconductors are divided into two groups, which are intrinsic and extrinsic semiconductors. Intrinsic semiconductors have extremely pure forms. In the lattice structure, the valence electrons tend to share with one of its valence electrons with each of its nearest neighbor atom and share one of its electrons from each neighbor atom. The shared electron pairs form covalent bond or valence bond. At low temperatures, the bonds are intact and rigid. At high temperatures, electrons break away due to the thermal energy they acquire. The thermal energy ionizes some atoms in the crystalline lattice and creates a vacancy in the bond. The neighborhood from which the free electron has come out leaves a vacancy with an effective positive charge which is known as the hole.

- At $T = 0$ K, an intrinsic semiconductor will behave like an insulator.
- At $T > 0$ K, the thermally excited electrons formed due to the thermal energy at high temperatures partially occupy the conduction band.

In extrinsic semiconductors, an impurity with a vacancy higher or lower than the vacancy of the semiconductor atoms is deliberately introduced, thereby drastically influencing the electrical properties of the semiconductor. Depending upon the type of impurity the semiconductors are divided into two groups, which are n-type and p-type semiconductors.

2.2. Metal Oxide Semiconductors

Metal oxide semiconductors (MOS) are the most commonly used sensing materials. These types of sensors are chemiresistive gas sensor. Metal oxides which behave like semiconductors have a high band gap resulting from their stoichiometry. It's constructed from two parts. Nanostructured metal oxide semiconductor gas sensors provide many advantages due to their low-cost, small dimensions, high sensitivity, and wide range of gas detection covering the oxygen, inflammable gases, and toxic gases.

Gas sensors based on metal oxide semiconductors have gained an increasing interest due to their characteristics. Devices based on MOSs have encumbrance, easy usage, low-cost, reliability, high-sensitivity and repeatability.

The most common sensitive MOSs in the gas sensing applications are n-type metal oxides (e.g. ZnO, SnO₂, etc.). On the other hand, much research has begun to focus on the p-type materials like Cr₂O₃ [17] and a few kinds of NiO_x [18, 19].

As it was mentioned in the gas sensor history, first metal oxide gas sensor based on ZnO developed by Seiyama, T. in 1962. Since then, there are many metal oxides became part of the gas sensor applications such as SnO₂, ZnO, Al₂O₃, Co₃O₄, NiO, CuO, Cr₂O₃, In₂O₃, WO₃, Fe₂O₃, TiO₂, V₂O₃, GeO₂ and Mn₂O₃ [20].

The most frequently used metal oxides in the gas sensor applications are shown as a chart with their percentages in the Fig. 2.4 since 2002 [21]. In the figure, It can be seen that, both ZnO and SnO₂ are the commonly used materials by %32. After these two materials In₂O₃ comes as a third material with the %10, then TiO₂ with %8 and WO₃ with %5, Fe₂O₃ and Ga₂O₃ with %4, CuO with %3 and finally NiO and V₂O₃ stays at the end with %1. These MOSs have a very important role in the environmental monitoring, chemical process controlling, personal safety [22], industrial process control, detection of toxic environmental pollutants on human health, prevention of hazardous gas leaks [23], wine quality monitoring, and traffic safety [24].

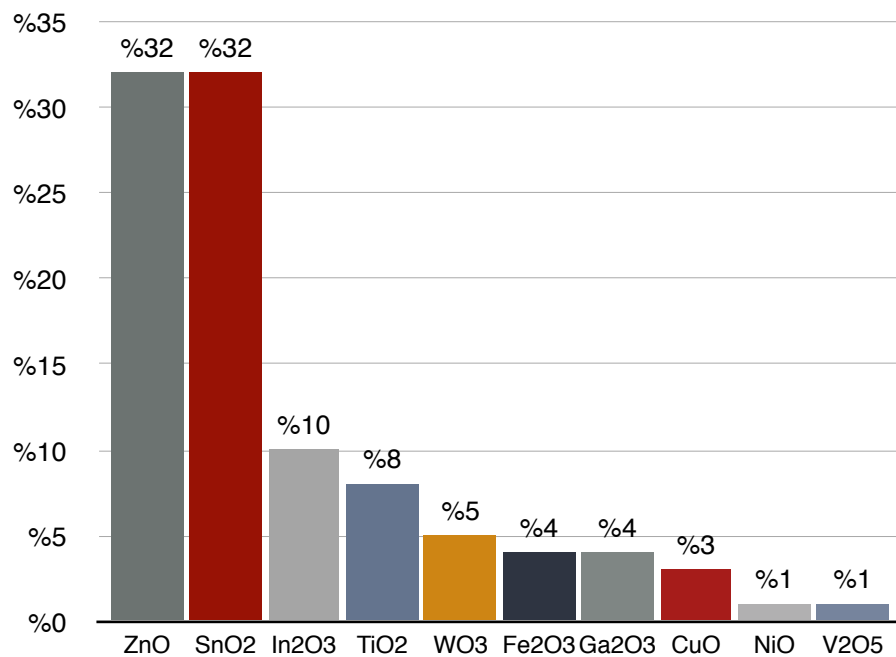


Figure 2.4 Top 10 metal oxide nanostructured materials used for gas sensor applications in publications since 2002.

Generally, metal oxides can be classified into two types according to their electronic structure:

- Transition-metal oxides (Fe_2O_3 , NiO , Cr_2O_3 , etc.)
- Non-transition metal oxides which include (1) pre-transition-metal oxides (Al_2O_3 , etc.) and (2) post-transition-metal oxides (ZnO , SnO_2 , etc.).

There are also many studies on composite materials in the gas sensor applications, such as SnO_2 - ZnO [25], Fe_2O_3 - ZnO [26], ZnO - CuO [27], etc. Composite gas sensors show higher sensitivity than the sensors produced with single material. For instance, SnO_2 - ZnO shows significantly responsive properties in sensing of ethanol, hydrogen [28, 29]. ZnO and TiO_2 compounds also make reactive composites. TiO_2 improves the gas sensing properties of sensors. Zhu, B.L., et al. report that the additive TiO_2 to ZnO greatly improves the sensitivity to VOCs [30].

In the Table 2.1, many metal oxides are listed in the gas sensing applications according to structure, synthesis method and target gas. As it can be seen that there are many routes for growth ZnO in gas sensor applications for many different target gases with SnO_2 . In the table, there is also Al_2O_3 , Fe_2O_3 , In_2O_3 , TiO_2 metal oxides and SnO_2 - ZnO , Fe_2O_3 - ZnO composites according to their synthesis methods and their structures. In the table, the most common target gas is CO after that ethanol is placed. The first ZnO gas sensor report is made by Wang, J.X., et al. in 2006. They fabricated ZnO nanorods on ZnO thin film by hydrothermal method using silicon wafer with a SiO_2 insulating layer as a substrate and operated the device as a gas sensor by targeting H_2 , CO and NH_3 . They fabricated ZnO nanorod array by preparing mixing appropriate quantities of ammonia (25%) and 0.05 M zinc chloride solution in a bottle. Then, they immersed Si substrate vertically in the

solution, sealed the bottle and heated to 90 °C for 4 h in an oven. The nanorods they fabricated have a diameter of 30–100 nm and a length of about several hundred nanometers.

Table 2.1 Research papers focusing on nanoscale metal oxide semiconductor gas sensors.

Material	Structure	Synthesis method	Target Gas	Ref.
ZnO	Nanorod	Hydrothermal	Hydrogen, Carbon Monoxide, Ammonia	[73]
ZnO	Nanorod	Sonochemistry	Carbon Monoxide	[53]
ZnO	Nanorod	Hydrothermal (autoclave)	Ethanol	[74]
ZnO	Thin film	Dip-casting	Hydrogen, Methane, Hydrogen Sulfide	[75]
SnO ₂	Nanowire	Electrodeposition	Carbon Monoxide	[76]
SnO ₂	Thin film	RF sputtering	Nitrogen Dioxide	[77]
Al ₂ O ₃	Thin film	Electrochemical Anodization	Humidity, Methane, Ammonia	[78]
Fe ₂ O ₃	Nanorod	Hydrothermal	Ethanol	[79]
In ₂ O ₃	Nanowire	Laser Ablation	Nitrogen Dioxide	[80]
TiO ₂	Nanotube	Electrochemical Anodization	Formaldehyde, Ethanol, Ammonia	[81]
SnO ₂ -ZnO	Microstructure	Sintering	Carbon Monoxide	[25]
Fe ₂ O ₃ -ZnO	Nanorod + Core shell	Three-step Process	Ethanol	[26]

2.2.1. Adsorption Mechanism of Metal Oxide Gas Sensors

The first interaction between the surface of metal oxides and gas molecules is physisorption (physically adsorption). Physisorption occurs by the rules of Van Der Waals. Then electron exchange starts to form between the gas molecules and semiconducting metal oxide surface. The process which the electrons in adsorbed gas molecules begin to fill the holes in the semiconducting metal oxide is called chemisorption

(chemical adsorption). Chemisorption occurs when there is the formation of a chemical (often covalent) linkage between adsorbate and substrate and takes shape exothermically.

In the MOSs, the mechanism of gas sensing depends on the reaction between the agents such as (O^-), (O^{2-}), (H^+), (OH^-) and the target gas molecules to be sensed, which is a redox (reducing/oxidizing) process. Target gas species are divided into two groups: oxidizing gas or electron acceptors such as O_2 , CO_2 and reducing gas or electron donor such as CO , $CHCl_3$ and ethanol.

Since, the chemical reaction is resulted from change of the carrier concentration in the conductivity, sensor resistance also changes and sensor resistance depends on a type of the MOSs. When an n-type MOS chemisorbed a reducing gas, the surface of the material provides extra electrons. Consequently, the resistance of n-type material is decreased. In the p-type MOS, the resistance of the surface is increased. The response of MOS under reducing and oxidizing gases is summarized in Table 2.2. The change of the sensor resistance on the exposure to the target gas (reducing gas) in the cases of n-type and p-type MOS sensors is illustrated in Fig. 2.5 [31].

Table 2.2 Resistance change in gas types [16].

Classification	Oxidising Gases	Reducing Gases
n-type	Resistance increase	Resistance decrease
p-type	Resistance decrease	Resistance increase

When the gas molecules have been pumped, they generate some pressure in the adsorption process. This partial pressure is changing according to the gas type, and each gas has different oxidation rates. If the partial pressure is low, Henry's law will occur. Henry's law says that the solubility of a gas is directly proportional to the pressure of that gas.

It means that the value of the physical adsorption is related to the partial pressure. If the tensile energy is higher than the energy of chemical adsorption, this process doesn't occur. The operating temperature of metal oxides is important because of different temperatures, adsorption process may break down. The existence of chemisorption implies the presence of a surface charge depends on Fermi - Dirac statistics.

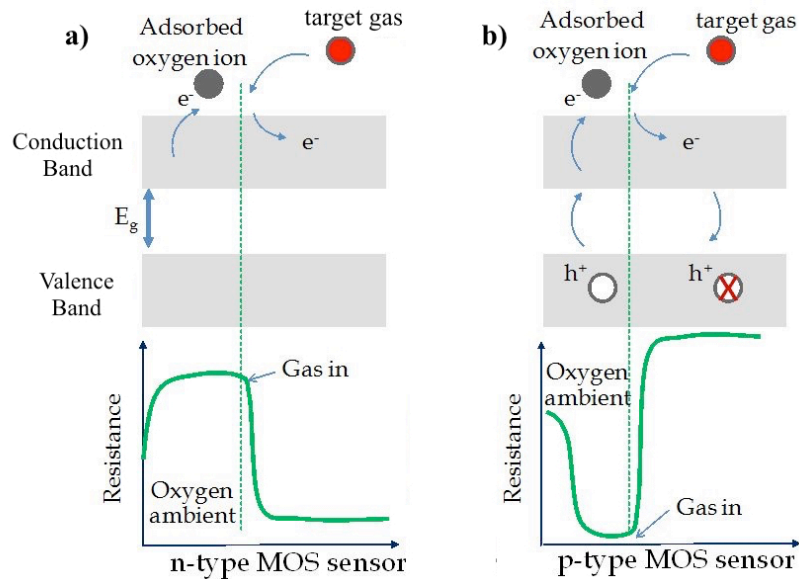


Figure 2.5 Schematic diagrams of resistance change of, a) n-type and b) p-type MOS under reducing gases.

During the interaction between the reducing gas and the surface with oxygen, a charge layer occurs on the surface and generates an electric field. Then, it causes a twisting on the energy band, when the surface charge is negative, it's upward twisting. This process causes an increasing in electrical resistance [10].

So far, we consider the conductivity between the nanorods of MOS, but every nanorod has its own conductive channel. Therefore, the sensor resistance needs to be contributed from two parts; (a) the resistance along a cylindrical nanorod; (b) the resistance between nanorods. The resistance along the nanorod is due to the widths of surface depletion layer and conductive channel.

According to the depletion layer model, L_d (Debye length), can be expressed by;

$$L_d = (\epsilon \times k_B \times T / q^2 \times n)^{1/2} \quad (2.1)$$

Where, ϵ is a static dielectric constant, k_B is the Boltzmann constant, T is the operating temperature, q is an electrical charge of a carrier, and n is a carrier concentration. According to this model, at steady operating temperature, the Debye length depends only on the carrier concentration. If we consider the Eq. (2.1) in the pure MOS nanorod sensor at the optimum operating temperature, the L_d can be regarded as a constant value and equals to a value of the depletion layer width. In this model, conductive channel of a nanorod is assumed to be along the axis of the nanorods. Conductive channel is also related with the carrier concentration [31].

When the sensing layer is exposed to the target gases which are reducing gas, gas reacts with oxygen ions of the MOS sensing layer and gives back electrons to the nanostructures of the MOS sensor resulting as increasing in the conductive channel which leads decreasing depletion layer width. This phenomenon is caused by increasing resistance and shown in Fig. 2.6 [31].

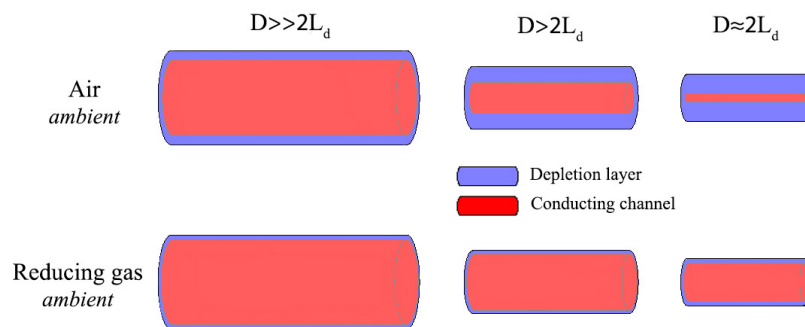


Figure 2.6 Schematic diagram of the depletion layer on the surface of cylinder with a thickness (or width) of L_d , under condition of $D \gg 2L_d$, $D > 2L_d$, and $D \approx 2L_d$.

2.3. Zinc Oxide (ZnO)

Zinc Oxide (ZnO) is an important semiconductor studied for many decades for different applications due to its excellent sensitivity, high electron mobility, good transparency, strong room temperature luminescence, versatility, reliability, and extreme low-cost. ZnO has an extensive range of properties, tunable conductivity from metallic to insulating, excessive transparency, piezoelectricity, wide band-gap, room temperature ferromagnetism, and huge magneto-optic, and chemical-sensing [32]. Conductivity is related to a stoichiometric excess of zinc ions, which occupy interstitial locations in the crystal lattice. Doping by the other elements to replace either the zinc or the oxygen, the conductivity can be varied over a very wide range. There are a lot of nanostructures of ZnO include nanowires, nanobelts, nanorods, nanotubes and nano-tetrapods.

The electrical properties of ZnO nanostructures are important for developing ZnO applications, especially in nanoelectronics. ZnO nanowires and nanorods are carried out in the electrical transport measurements. ZnO is a semiconductor which has a wide direct band gap of 3.37 eV and large excitation binding energy of 60 meV at room temperature. Because of this, it has advantages in high breakdown voltages, ability to sustain massive electric fields, low electronic noise, high-temperature, and high-power operation. ZnO has a maximum of ~ 2000 ($\text{cm}^2 \times \text{V}^{-1} \times \text{s}^{-1}$) electron mobility at 80 K. Hole mobility values vary in the range of 5-30 ($\text{cm}^2 \times \text{V}^{-1} \times \text{s}^{-1}$). Most of ZnO structures show n-type semiconductor behavior. Many applications of ZnO still remain with the difficulty of p-type doping especially in the applications of electronics and photonics. Since, p-type dopants have low solubility. P-type and n-type ZnO nanowires can be used as p-n junction diodes and LEDs. Physical properties of ZnO are listed in Table 2.3.

ZnO has been the subject of intensive research applications for ultraviolet (UV) light emitters, short-wavelength nano-lasers, piezoelectric devices, ultra-sensitive spin electronics, field-effect transistors, and field-effect emitters.

Table 2.3 Basic properties of ZnO .

Properties of ZnO	
Crystal Structure	Hexagonal, Wurtzite
Molecular Weight	Zn:65.38, O:16 and ZnO:81.38
Lattice Constant	$a = 3.246 \text{ \AA}$, $c = 5.207 \text{ \AA}$
Density	5.67 g/cm ³ or 4.21×10^{19} ZnO molecules/mm ³
Cohesive Energy	$E_{\text{coh}} = 1.89 \text{ eV}$
Melting Point	$T_m = 2250 \text{ K}$ under pressure
Heat of Fusion	4, 470 cal/mole
Thermal Conductivity	25 W/mK at 20 °C
Thermal Expansion Coefficient	$4.3 \times 10^{-6} / \text{K}$ at 20 °C, $7.7 \times 10^{-6} / \text{K}$ at 600 °C
Band Gap at RT	3.37 eV
Refractive Index	2.008
Electron and Hole Effective Mass	$m_e^* = 0.28$, $m_h^* = 0.59$
Debye Temperature	370 K
Lattice Energy	964 kcal/mole
Dielectric Constant	$\epsilon_0 = 8.75$, $\epsilon_\infty = 3.75$
Exciton Binding Energy	$E_b = 60 \text{ meV}$
Piezoelectric Coefficient	$D_{33} = 12 \text{ pC/N}$

2.3.1. Crystal Structure

Group II-VI elements crystallized in cubic (zinc-blende) or hexagonal (wurtzite) structures. In both crystal structures, the zinc and oxide centers are tetrahedral and four cations surround the anions at the corners of a tetrahedron. They establish a typical sp^3 covalent bonding, but they have also substantial ionic character.

ZnO compound as well is in the group II-VI of periodic table, and its ionicity occurs at the border between covalent and ionic semiconductor. Since oxygen was classed as an element of 6A group and zinc is a member of the 2B of the periodic table. ZnO generally has a hexagonal wurtzite structure in the nature, and this structure is the most stable form at ambient conditions, which is shown in Fig. 2.7. Hexagonal wurtzite structure has resistance against the thermodynamic changing. Other crystal structures have resistance to special conditions like pressure.

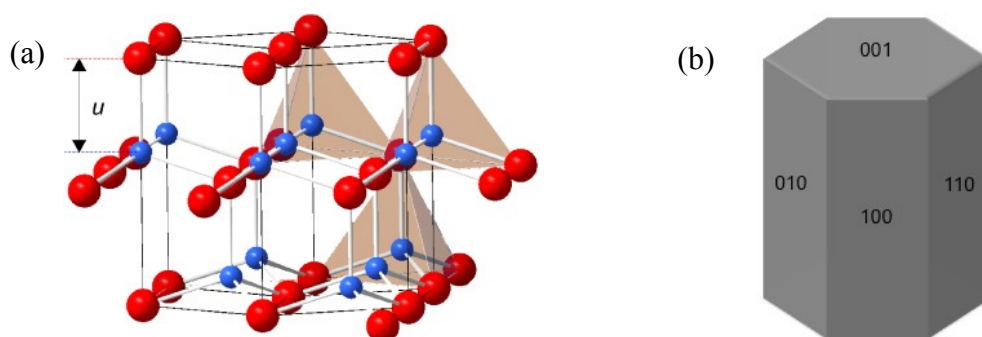


Figure 2.7 (a) The hexagonal wurtzite structure of ZnO. The O-atoms are the large red spheres and the Zn-atoms are the small blue spheres [100]. (b) Hexagonal faces of wurtzite ZnO nanorod with c-axis [001] orientated growth [102].

ZnO has polar, semi-polar and non polar surfaces, the polar Zn (0001) and O (0001) terminated faces and the semi-polar (1120) and (1010) faces. The semi-polar surfaces contain equal numbers of Zn and O atoms [33]. The ZnO wurtzite structure has a hexagonal closed-packed unit cell, and the dimensions $a = b \cong 0.3249$ nm and $c \cong 0.5206$ nm at room temperature.

2.3.2. Gas Sensing Properties of ZnO

ZnO is one of the primary material that is used in the gas sensing applications. Oxygen vacancies of ZnO are electrically and chemically active. These vacancies work as n-type donors, so they increase the conductivity of ZnO significantly. ZnO nanostructures exhibit greater

sensitivity and faster response than their bulk counterparts. The main gas sensing parameters are sensitivity, response time, recovery time, detection range, and optimum working temperature. Primarily, sensitivity of the ZnO nanostructured gas sensors depend on the working temperature. For instance, when oxygen molecules trap electrons on the surface to produce (O^{2-}), at low temperatures (under 150 °C), (O^-) and (O^{2-}) are the predominant oxygen molecules at higher temperatures (150 – 450) °C [34]. Sensitivity is also related to the target gas concentration, i.e., the resistivity of 1-D ZnO nanostructure increases by the expanding target gas concentration. ZnO nanowires and nanorods have a very substantial surface-to-volume ratio which enhances the gas sensing performance.

ZnO nanostructures form in the different surface states, size and morphology, based on the growth technique. The properties and performance of ZnO nanostructures could be effected by these parameters. For instance, the surface roughness enhances the sensitivity of ZnO nanorods. Wang, C.H., *et al.*, presented this information in the hydrothermally growth of ZnO nanorods [35]. The reason for high sensitivity is the surface roughness which provides more active sites to target gases on the surface of the sensing structures.

2.3.3. Growth Techniques For ZnO

Various growth techniques employed for the growth of ZnO. These techniques are categorized as; (a) wet processing, (b) solid-state processing and (c) vapor-phase processing routes. Wet processing routes include hydrothermal and sonochemistry techniques to grow ZnO nanoparticles in an aqueous solution. Carbothermal reduction and solid-state chemical reaction techniques are utilized in solid-state processing routes for the growth of ZnO. Molecular-beam epitaxy (MBE), RF (Radio Frequency) sputtering, aerosol, thermal evaporation and chemical

vapor deposition (CVD) techniques are used in the vapor-phase processing routes to grow ZnO nanostructures [36].

2.3.3.1. Hydrothermal

Generally, the word of “hydrothermal” is used in the geology. It is known as a hydrothermal circulation, which relates to or denotes the action of heated water in the Earth’s crust. When the sea water is mixed with the stream of hydrothermal fluid, it becomes to formate many minerals under high pressure and temperature within the crust. This process is adapted to the chemistry in growth of the nanostructures.

The working principle of hydrothermal technique depends on the solubility of minerals in hot water under high pressure, and it is used in the synthesis of single crystal materials. This method has been used in the growth of crystal materials since 1970. The growth is performed in an apparatus within an autoclave, in which a nutrient is supplied along with water. The temperature of the system is maintained between the opposite points of the growth chamber. At the hottest point the nutrient solute dissolves while at the coolest point, it is deposited on a seed crystal. Hydrothermal technique is the most applied synthesis technique to grow nanostructures of ZnO. Because it is relatively simple compared to other growth techniques. Hydrothermal process relies on the reaction between the solutions containing a zinc source usually zinc acetate, zinc nitrate and zinc chloride, etc. with the solution containing reducing agents such as sodium hydroxide and ammonium nitrates. As an example in the literature, *Liang, S., et al.* fabricated flower-like and rod-like microstructures by microwave assisted hydrothermal method, which is extracted at different stages of the reactions: (a) precursor preparation, (b) microwave irradiation heating, and (c) natural cooling [37].

2.3.3.2. Carbothermal Reduction and Solid-State Chemical Reaction

Carbothermal reduction method is a single-step method, and it uses the reduction of metal oxides by employing activated carbon (C) as a reduction agent. In the chemical reaction of carbothermal reduction, the temperature needs to be increasing in every minute until it reaches to 350–1600 °C. When the desirable temperature maintained, the reaction cools down to the room temperature. Carbothermal reduction method is one of the good candidates in the growth of ZnO. There are some examples in literature, which *Tharsika, T., et al.* fabricated ZnO/SnO₂ blended nanowires, which have 15-80 nm diameter length ranging from 2 μm to several tens of micrometers by carbothermal reduction of mixed ZnO and SnO₂ powders with activated carbon under atmospheric pressure on a gold (Au) coated alumina substrate [38].

Solid-state chemical reaction provides a relatively simple method, which does not require high temperature, and it can be used for mass production of ZnO nanorods. The typical procedure of this technique is, as reported in *Hou, X., F. Zhou, and W. Liu*, anhydrous ZnSO₄ and NaOH were blended together in an agate mortar and ground thoroughly for 20 min under the irradiation of an IR lamp [39].

2.3.3.3. Molecular-Beam Epitaxy (MBE)

The word of epitaxy means surface arrangement. Therefore, it deals with the ordered placement of atoms on the surface. MBE is invented in the late 1960s at Bell Telephone Laboratories®. Since then, it is widely used in the production of semiconductor devices, including transistors for cellular phones and WiFi.

MBE is a technique to grow crystalline thin films in high vacuum or ultrahigh vacuum (UHV) (10⁻⁸ Pa) with precise control of thickness,

composition and morphology. Deposition rate is the most important aspect of the MBE in control of the deposition, which is less than 3000 nm per hour. This deposition rate allows the films to grow epitaxially. The highest purity and defect-free grown films are resulted in the UHV environment in the absence of a carrier gas. Reflection high energy electron diffraction (RHEED) is used for monitoring the growth of the crystal layers during the process. The shutter in front of each furnace is controlled by a computer down to a single layer of atoms as well as allowing to manage of the thickness of each layer. *Heo, Y.W., et al.* reported ZnO thin film by MBE on Al₂O₃ wafer substrate using ozone/oxygen mixture as an oxidizing source at 350 °C. Their vacuum pressure of the growth chamber was $\sim 5 \times 10^{-8}$ mbar [40].

2.3.3.4. RF Sputtering

Sputtering is one of the most popular growth techniques in the deposition of ZnO thin films and there are three types of sputtering (a) DC sputtering, (b) RF sputtering, and (c) reactive sputtering. RF sputtering is the preferred one in these techniques because of its cost-efficient, simplicity, and low operating temperature. ZnO thin film deposition occurs at a certain substrate temperature via ejecting high-pure ZnO atoms and coat onto the substrate such as silicon wafer or glass using RF sputter system in the atomic level by bombardment with high-energy particles. First, a gaseous plasma is produced. The plasma is assembled from the alternating signal when it is applied to the cathode, and then, ions from this plasma are removed and sent through into source material. These removed ions abrade the source material via energy transfer and produced particles from the source material as a form of neutral particles. These particles travel in a straight line through the substrate, and the substrate would be deposited. The deposition is usually carried out in pressure of $10^{-3} - 10^{-2}$ Torr with O₂ (as a reactive gas) and

Ar (as sputtering enhancing gas) ambient in a vacuum chamber. RF sputtering systems use a high-frequency generator, typically use 13.56 MHz for generating electromagnetic power. RF sputtering only occurs in the extremely high (or much higher than normal thermal energies) kinetic energy of the bombarding particles.

There are several advantages of RF sputtering. First, It is very suitable with insulating targets. The driving RF frequency changes the sign of the electric field at every surface in the chamber. So, it protects charge-up effects and reduces arching. RF sputtering doesn't need magnetic confinement. So, it provides optimum coating uniformity, no poisoning of the target, a few or no arching and a more stable process. RF sputtering does not show disappearing anode problems. In RF sputtering, when ions are too heavy in the RF system because of different masses, electrons can be accelerated to oscillate with the RF [41].

There are many examples of grown ZnO thin film by RF sputtering technique for the gas sensing applications. For example, *Al-Hardan, N.H., et al.* deposited ZnO thin films by reactive RF sputtering on the thermally oxidized silicon wafer for the sensing of acetone, isopropanol and ethanol. The grown ZnO thin film has a thickness of 250 nm and total area of $2 \times 2 \text{ mm}^2$ [42].

2.3.3.5. Aerosol Deposition

Another method in the vapor-phase process is aerosol deposition technique. Aerosol is a deposition technique to growth dense films based on the impact and consolidation phenomenon of particles at room temperature. In the aerosol deposition, a few hundred meters per second accelerated particles are carried by a carrier gas and directed through a nozzle onto a substrate. It is possible to deposit thin films on metal, glass

and ceramic substrates by aerosol. A research paper on the growth of ZnO nanoparticles by aerosol method is reported by *Ozcelik, B.K. and C. Ergun*. They produced ZnO nanoparticles by a spray pyrolysis method using the aerosol technique. They prepared a solution with Zinc nitrate hexahydrate in methanol at a concentration of 2.75 mol/L. They applied this solution to the substrate via spray pyrolysis and dried the sample at 70 °C followed by heat treatment at 600, 800 and 1000 °C for 1 h. [43].

2.3.3.6. Thermal Evaporation

One of the most common deposition techniques is thermal evaporation under high-vacuum environment. Thermal evaporation is very suitable for fabricating high-quality thin films with nanoscale thickness on glass, plastic films, metals, and almost any other kind of substrates. The purity of source material is very important for the deposition in thermal evaporation.

A 0.4 nm particle has a released path of 60 m at a pressure of 10^{-4} Pa, has a mean free path of 60 m. Therefore, vaporized particles travel directly to the substrate by high vacuum without colliding with the background gas. Then, they condense back to a solid-state on the substrate. Solid state material is almost entirely transmuted to vapor phase before the deposition. If there are other hot objects in the evaporation chamber such as heating filaments, there would be unwanted vapors that limit the quality of the vacuum. Thermal evaporators use an electron beam (e-beam) or resistive heating to evaporate the targeted materials. An e-beam can provide high melting points even above 2000 °C which is a very proper temperature for the purest thin films, especially for optical substrates, and it can provide many advantages in the control of deposition rate, excellent material utilization, sequential, co-deposition and uniform low temperature deposition.

There are many papers for the growth of ZnO nanostructures by this technique. One of these papers is prepared by *Fang, Y., et al.* They fabricated well-aligned ZnO nanowires on a bare glass substrate without the assistance of any catalysts by thermal evaporation technique. They studied the photoluminescence (PL) properties and growth mechanism of ZnO. They found oxygen flow rate is the substantial effect on the morphology of ZnO nanowires [44].

2.3.3.7. Chemical Vapor Deposition (CVD)

Chemical vapor deposition (CVD) is a chemical process that is used to produce high purity and high-performance single crystalline nanomaterials. Especially, CVD method is used in the semiconductor industry in the deposition of films. It is also used in optoelectronics applications, optical coatings, and coatings of wear resistant parts. The process of CVD occurs by volatile chemical precursors, which are transported in the vapor phase to react and/or decompose on a heated substrate to produce the desired nanostructures. It is possible to deposit many materials in monocrystalline, polycrystalline, amorphous, and epitaxial forms depending on the materials and reactor conditions with CVD. A typical CVD process has a complex motion dynamics because of the flowing gases into the chamber.

CVD has many advantages just like molecular-beam epitaxy and RF sputtering. First of all, CVD allows coating of three-dimensional structures with large aspect ratios based on the pressure of high vacuum. Second, extreme precursor flow rates provide higher deposition rate in CVD, and its reactor can be scaled to fit multiple substrates. CVD does not require UHV but there are some CVD systems that use UHV and changes and additions the precursors are very simple. Besides, CVD has the ability of fabricating abrupt junctions.

However, there are some disadvantages of CVD technique. First, high temperatures in the deposition, which is greater than 600 °C, can damage structures already fabricated on substrates. Another is that many precursors used in the CVD systems are hazardous or poisonous. So, the devices, made by these precursors, may also be toxic. Therefore, some precautions have to be taken in the treatment of the reactor exhaust and the precursors. The other one is the many precursors, especially the metal-organics, require high-cost [45]. The working principle of CVD is given in the Fig. 2.8.

Chien, F.S.-S., et al. fabricated ZnO nanorods by CVD and used the device in sensing application. They studied ozone sensing properties of ZnO nanorods. They measured the response time, recovery time and sensor response to ozone. They observed flowerlike nanorods by these characterization techniques [46].

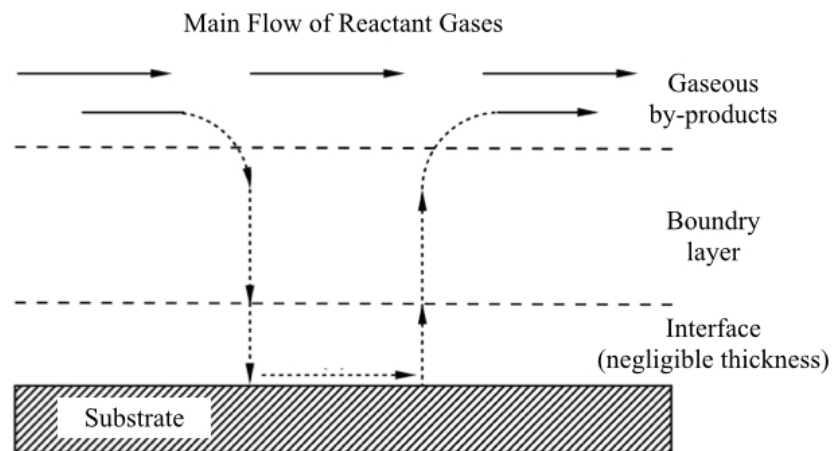


Figure 2.8 Working principle of CVD .

The list of research papers of ZnO nanostructured gas sensors are given in Table 2.4. They are separated according to growth technique for nanostructures, target gases and measurement type. The primary applied measurement system is conductivity, then Quartz Crystal Microbalance (QCM) is used, and the most operated growth technique is the hydrothermal method in ZnO.

Table 2.4 Research papers focusing on nanoscale zinc oxide (ZnO) gas sensors.

Growth Technique	Nanostructure	Target Gases	Measurement Type	Ref.
Hydrothermal	Nanowire	Carbon Monoxide	Conductivity	[82]
Thermal Evaporation	Nanowire	Ammonia	QCM	[83]
Hydrothermal	Flower-like nanorod	Sulfur Dioxide, Thionyl Fluoride, Sulfuryl Fluoride	Conductivity	[84]
Hydrothermal	Nanorod	Hydrogen, Methane, Ammonia, Ethanol, Hydrogen Sulfide	Conductivity	[35]
Wet Chemical Method	Thin Film	Amine Gases	PL spectra	[85]
MicroElectroMechanical System (MEMS)	Nanowire	Ethanol	Conductivity	[86]
Wet Chemical Method	Nanorod	Ammonia	QCM	[87]
Carbothermal Catalyst-Free Vapor Solid (VS)	Nanowire	Humidity	QCM	[88]
Hydrothermal	Nanorod	Ethanol, Formaldehyde, Ammonia, LPG, Gasoline	Conductivity	[74]
RF Sputtering	Thin Film	Acetone, Isopropanol, Ethanol	Conductivity	[42]
Sonochemistry	Nanorod	Carbon Monoxide	Conductivity	[53]
Self-Catalyzed Vapor-Liquid-Solid (VLS)	Nanowire	Carbon Monoxide	Conductivity	[89]
Hydrothermal	Nanorod	Ethanol	Conductivity	[90]

2.4. Sonochemistry

Sonochemistry utilizes the ultrasound to create a unique environment for the chemical reactions. Sonic spectrum has wide-range frequency. Humans can hear in the 20 Hz - 20 KHz frequencies. Ultrasound is above these frequencies and covers the range from 20 kHz up to 200 MHz. Sonochemistry is used in the range of 20 kHz - 2 MHz frequencies. The configuration of the sonic spectrum is shown in Fig. 2.8. Sonochemistry deals with the effect of sonic waves and properties of these waves.

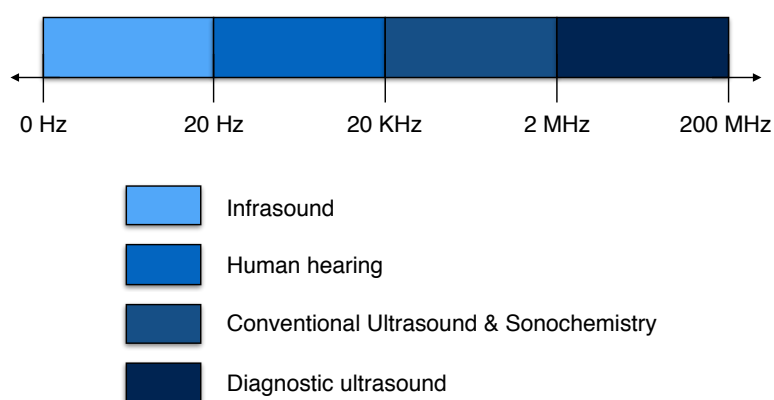


Figure 2.9 Frequency range of sound.

Ultrasound does not make a direct contact with molecules of the materials. Sonochemistry occurs with the acoustic cavitation which forms, grows and implodes of bubbles in a liquid environment.

As it was mentioned before, sonochemistry alternates expansion and compression by the acoustic cavitation. Acoustic cavitation creates bubbles, and these bubbles oscillate and accumulate under ultrasonic energy and grow until they reach an unstable size. When these bubbles reach to variable size, they eventually implode and release an extreme localized energy. This collapse occurs in less than a nanosecond with very massive temperature of ~ 5000 K and pressure of ~ 1000 atm, with high heating and cooling rate above 10^{11} K/s. This local energy is called

hot spot and chemical reactions can be occurred by these hot spots, which are not accessible within a nanosecond [47]. The illustration of this phenomenon is shown in Fig. 2.9. Sonochemical method was found to be feasible as it does not require complex setup. It does not produce any hazardous wastes, accordingly it is not harmful to the environment.

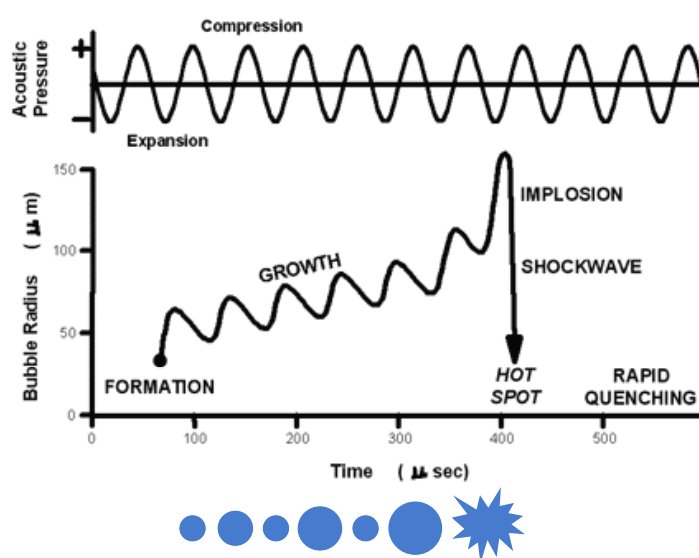


Figure 2.10 The illustration of acoustic cavitation.

There are many techniques to grow nanostructures. However, sonochemical method is primary on the growth of some materials. Amorphous products can be obtained by sonochemically [48]. Sonochemical method does not require glass formers in the mixture and also produces at the nanoscale. Sonochemistry is used to add amorphous nanosized catalysts into the mesopores. The nanoparticles can be deposited as a layer on the inner mesopores [49]. Sonochemistry is also employed in the growth of many nanomaterials such as metals, metal oxides, semiconductors on the surfaces of ceramics and polymeric materials [50, 51]. Sonochemistry is also used in the formation of micro and nano spheres of proteins [52].

One of the sonochemistry research papers is published by *Eugene, O. and J. Soo-Hwan*. They fabricated ZnO nanorod gas sensors via a

sonochemistry and studied their gas sensing characteristics for CO gas by varying the diameter of the nanorods. They deposited interdigitated comblike Pt electrodes on the substrate by DC sputtering and Zn thin-film using the RF sputtering. They used 0,1 M zinc nitrate hexahydrate (ZNH) and hexamethylenetetramine (HMT) solutions [53].

The research papers focusing on the sonochemistry are given in the Table 2.5 according to material, structure and application. It can be seen that both organic and inorganic nano and micro materials can be synthesized by the sonochemical method, and these materials can be used for many applications. Some of the given applications in the table are super capacitors, gas sensors, solar cells, photodetectors and lithium batteries.

Table 2.5 Research papers focusing on the sonochemical growth.

Material	Structure	Application	Ref.
Albumin and Haemoglobin	Microspheres	Characterization	[91]
MnO₂	Nanostructure	Super capacitor	[92]
ZnO	Nanorod	Gas Sensor	[93]
Pt, Au and Pd	Nanoparticle	Photocatalytic Production	[94]
TiO₂	Mesoporous	Dye-Sensitized Solar Cells	[95]
SnO	Nanocrystalline	Rechargeable Lithium Batteries	[96]
Fe₃O₄	Magnetic Nanoparticle	Catalytic Removal of Organic Pollutants	[97]
ZnO	Nanorod	Gas Sensor	[53]
ZnO	Hollow Spheres	Dye-Sensitized Solar Cells	[98]
ZnO	Nanowire	UV Photodetector and Gas Sensor	[99]

3. EXPERIMENTAL

In order to examine the electrical properties of the ZnO molecules and increase the quality of the signal, gold (Au) interdigitated electrodes (IDE) were deposited on the glass substrates by photolithography method. Later, sonochemistry was employed for the synthesis of ZnO within a short period of time. Using 400 W ultrasonic probe working at 24 KHz (HEILSCHER® UP 400S), a continuous seed-layer was first deposited over the glass substrate followed by the growth of the nanorods to ensure stronger bonding of ZnO molecules and to make nanorods more permanent on IDE deposited glass substrate.

All chemicals used in this thesis were used directly without any further purification, and all preparations were done at room temperature.

3.1. Synthesis of ZnO Nanorod for Gas Sensor Application

3.1.1. Gold(Au) Electrode Deposition

In order to deposit electrodes, 26×20 mm² glass substrate was sterilized ultrasonically in acetone, ethanol, 2-propanol and deionized water for 15 minutes respectively and then substrate was dried via high-purity nitrogen gas. In the last step of sterilizing, substrate was bombarded with ionized Ar gas to be disinfected from the organic pollutants in the thermal evaporator which is NVTE 300 model and produced by NANOVAK® Corporation (plasma cleaning). The image of this thermal evaporator is shown in Fig. 3.1.

Gold electrodes deposited on the glass substrate ~20 nm thickness chromium film to prevent the desorption of gold film from the surface of the substrate. Chromium (Cr) makes stronger bonds with both glass and gold. Deposition of chromium film was made by the thermal evaporation deposition system. After cleaning procedure, glass substrate was placed

in the thermal evaporator to deposit Cr film. After that, 60 nm thickness Au film deposited on the chromium.



Figure 3.1 The image of the thermal evaporator.

All the experimental procedure to prepare electrodes was done in clean room, which is UV protected. For the next step, prepared gold film was coated with positive photoresist. Photoresist was added drop-wise on the gold film and stirred at 4600 rpm for 45 seconds in the spin coating device. After spin coating, substrate needs to be heated because, photoresist is liquid additive. So, substrate was heated at 90 °C for 50 seconds (soft bake). Then, substrate was placed in the mask aligner (Hydralign Series 2000, OAI®) properly, beneath the mask and was exposed the UV light for 3 seconds. The image of mask aligner is shown in Fig. 3.2. During this process, the portion other than the mask off, the chain between the molecules forming by the photoresist coating, is broken by UV light. So, the portions which can be reached by light,

contaminates and breaks. After exposure, substrate was placed in corrosive (AZ 726 MIF developer) which can remove broken molecules from the surface for 3 seconds and was dipped into the deionized water to prevent removal of unbroken molecules. Prepared substrate was dried under Ar gas.



Figure 3.2 The image of the mask aligner.

After this procedure, there was only gold film stayed on the substrate. This gold film was removed with aqua regia, which is 3 HCL: 1 HNO₃. This solution etches every gold particle it can reach. Then substrate was dried with Ar gas again. There is only Cr stayed on the surface. It was also etched from the surface by 1 HCL:1 H₂O solution and dried via Ar gas. Then, photoresist which stays on gold electrode pattern was etched from the surface of gold by acetone and dried via Ar gas. After all of these procedures, Au electrodes had been deposited on the glass substrate. IDE pattern contains 2 μm spacing, and this

interdigitated structure is placed in the tips of the pattern. This deposited electrode structure on the surface is illustrated in Fig. 3.3.



Figure 3.3 The illustrated figure of gold electrodes on the glass substrate.

3.1.2. ZnO Seeding Process

Deposition of seed layer is very pivotal in the sonochemical growth of ZnO nanorods. In the literature, many reports have shown that for ZnO nanorods to be obtained from a reaction between Zinc nitrate ($\text{Zn}(\text{NO}_3)_2$) and Hexamethylenetetramine ($\text{C}_6\text{H}_{12}\text{N}_4$), which will be referred as HMT. Seeding process is very uncomplicated and requires one-step implementation, which employs Zinc acetate dihydrate ($\text{Zn}(\text{CH}_3\text{COO})_2 \times 2\text{H}_2\text{O}$) for both polar and non-polar ZnO nanoparticles on a substrate.

Preparation of zinc (ZnO) seed layer is very simple on the surface of the glass substrate. A 0.005 M solution of Zinc acetate dihydrate in isopropyl alcohol was prepared by dissolving 0.55 g Zinc acetate dihydrate in a beaker containing 0.5 L Isopropyl alcohol at room temperature. The solution was stirred with a magnetic stirrer at 750 rpm for 15 min. Complete dissolve of zinc acetate dihydrate in isopropyl alcohol is difficult with the magnetic stirrer. Therefore, solution was placed in the ultrasonic processor and sonicated for 10 min at 50% of the maximum amplitude of the 24 KHz ultrasonic probe working at 400 W at 0,8 sec in one-second working time. When the Zinc acetate dihydrate is completely dissolved, a clear solution was obtained. Then the glass substrate was placed into the solution and sonicated for 30 min at

maximum amplitude of the 24 KHz ultrasonic probe working at 400 W at 0,8 sec in one-second working time. After the sonication, the sample was heated at 70 °C for 10 minutes on the heater to evaporate the liquid molecules. The illustrated configuration of seed layer on the surface is shown in Fig. 3.4.



Figure 3.4 The illustrated figure of seed layer on the glass substrate.

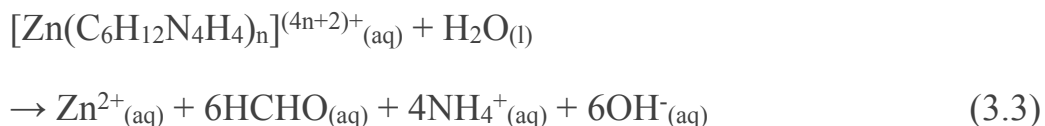
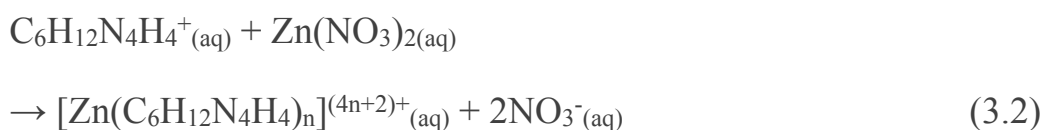
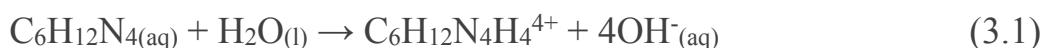
3.1.3. Growth Process

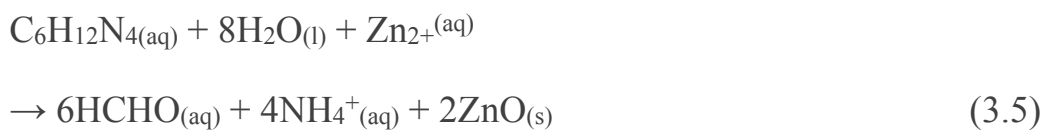
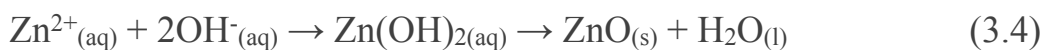
Growth of ZnO nanorods on a ZnO-seeded substrate is enabled with the reactions between HMT, and zinc nitrate under the effect of ultrasound. In order to grow ZnO nanorods, an aqueous solution of 0.04 M Zinc nitrate tetrahydrate ($\text{Zn}(\text{NO}_3)_2 \times 4\text{H}_2\text{O}$), and 0.04 M HMT ($\text{C}_6\text{H}_{12}\text{N}_4$) was prepared. First, 2.8038 g of HMT was dissolved in a beaker containing 0.5 L deionized water and stirred with a magnetic stirrer at 750 rpm for 10 min. In a separate beaker containing 0.5 L deionized water, 5.2288 g of $\text{Zn}(\text{NO}_3)_2 \times 4\text{H}_2\text{O}$ was dissolved and the solution was also stirred at 750 rpm for 10 min. Equal volumes of solutions were taken and placed in another beaker and stirred for 5 minutes. Then, the substrate was placed into the solution and sonicated under ultrasonic probe at maximum amplitude of the 24 KHz working at 400 W for 60 min at 0,8 sec in one-second working time. After the sonication, the sample was heated at 70 °C for 10 minutes on the heater, to evaporate the liquid remains on the surface. The image of ultrasonic processor is shown in Fig. 3.5.



Figure 3.5 The image of the ultrasonic processor set up.

When the prepared solution and glass substrate were placed under the ultrasonic processor, $\text{Zn}(\text{NO}_3)_2 \cdot 4\text{H}_2\text{O}$ and HMT start to interact with each other under extreme local temperature of ~ 5000 K and pressure of ~ 1000 atm, with high heating and cooling rate above 10^{11} K/s in the nanoscale based on the cavitation phenomenon. This energy keeps forging to the substrate continuously. Under this continuous local energy, ZnO nanoparticles begin to form and grow on the surface. HMT is an auxiliary chemical with $\text{Zn}(\text{NO}_3)_2 \cdot 4\text{H}_2\text{O}$ for ZnO. The reactions of $\text{Zn}(\text{NO}_3)_2 \cdot 4\text{H}_2\text{O}$ and HMT to form ZnO nanoparticles is given below [54];





At the end of these reactions, ZnO nanorods were formed. The structure of HMT ($\text{C}_6\text{H}_{12}\text{N}_4$) is shown in Fig. 3.6 and the illustration of ZnO nanorods on the surface is shown in Fig. 3.7 and growth nanorod process is shown in Fig. 3.8.

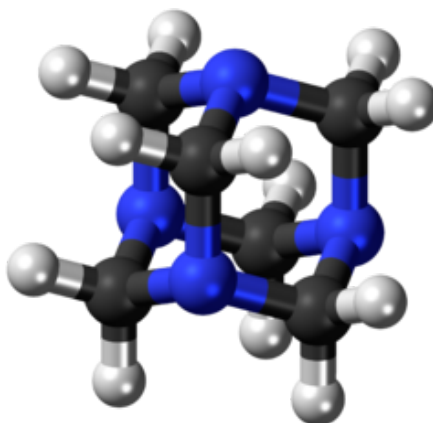


Figure 3.6 Structure of hexamethylenetetramine (HMT); blue spheres are nitrogen (N), black spheres are carbon (C) and white spheres are hydrogen (H) atoms [101].

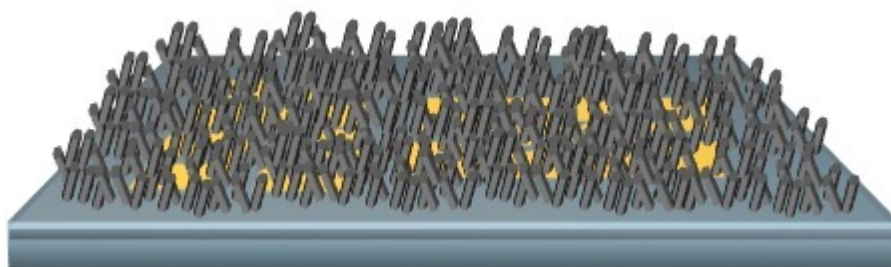


Figure 3.7 The illustrated figure of ZnO nanorod grown on IDE.

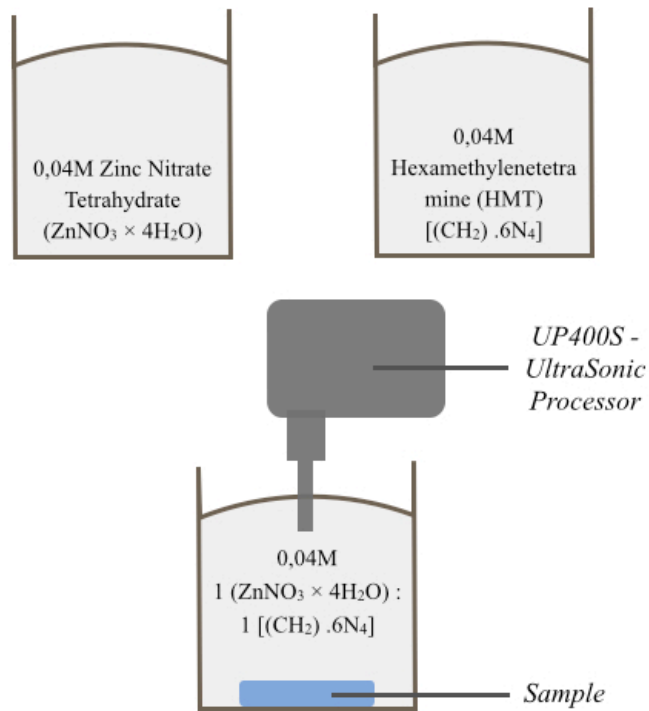


Figure 3.8 The illustrated figure of ZnO nanorod growth process, on the glass substrate.

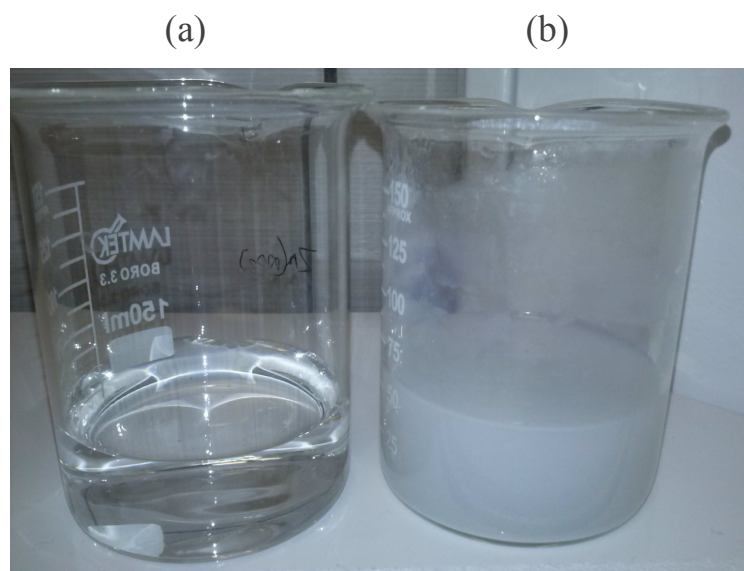


Figure 3.9 The image of ZnO growth mixture solution; (a) before sonication, (b) after sonication.

3.2. Characterization Techniques

Various techniques have been used for surface characterization and elemental analysis of the sonochemically synthesized ZnO nanorods. Specifics of the Scanning Electron Microscopy (SEM), Raman and Energy Dispersive X-ray Spectroscopies (EDS) are given below.

3.2.1. Optical Microscopy

The samples were characterized first with an optical microscope. Optic microscope uses visible light and a system of lenses to magnify particles of samples from 5x to 100x. The images from the optic microscope can be captured by light-sensitive cameras. However, in modern developments in CMOS (Complementary Metal-Oxide Semiconductor) and CCD (Charge-Coupled Device) cameras allow the capture of digital images, and the image is shown directly on a computer screen. There are two types of configurations of the optical microscope: the simple microscope and the compound microscope. In the basic microscope, a lens or set of lenses are used to enlarge an object through angular magnification alone. Compound microscope uses a lens close to the object being viewed to collect light, which is called as the actual lens focuses a real image of the object inside the microscope. Compound microscopes are in the majority of modern research.

Nikon® Eclipse LV150N optical microscope equipped with clemex captiva CCD camera and digital image analysis software, which is shown in the Fig. 3.10, is used for the first characterization of the samples.

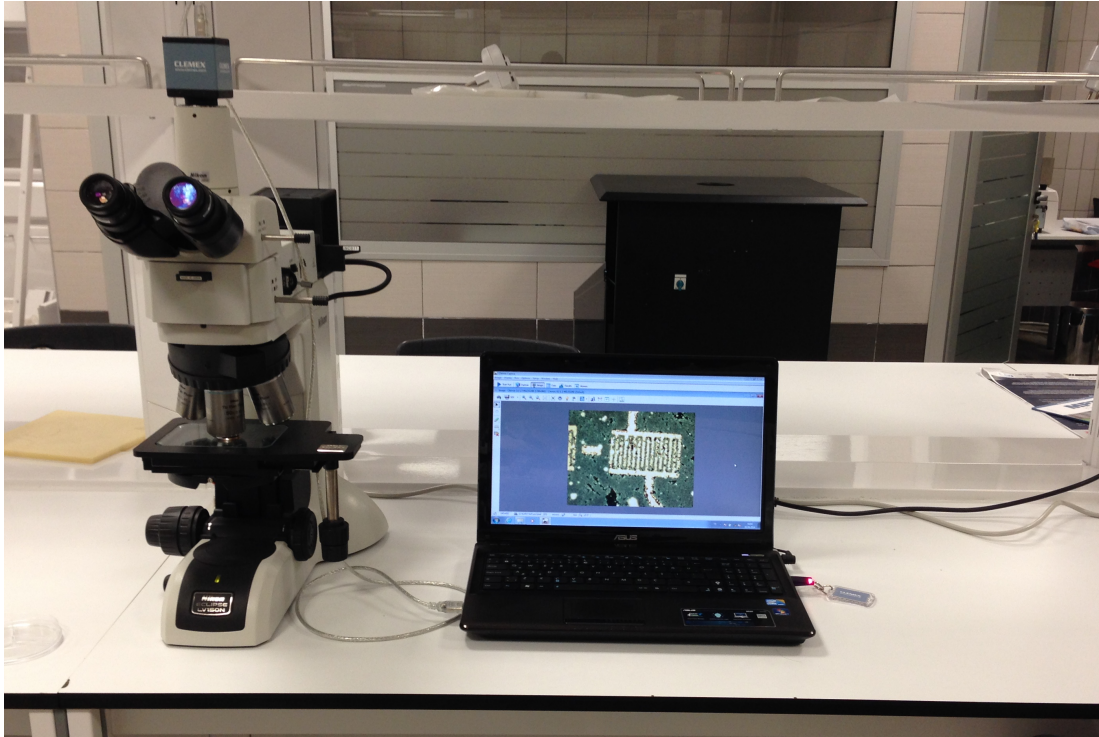


Figure 3.10 Optical microscopy system used for the thesis.

3.2.2. Scanning Electron Microscopy (SEM)

Scanning Electron Microscopy (SEM) provides detailed topographic features of the samples, including shape and size of particles. In a typical scanning electron microscope, sample is examined in a raster pattern with a focused beam of electrons, which is generally produced by either thermally or by field emission using Tungsten(W) filament or lanthanum hexaboride (LaB6) crystals.

There are two magnetic lenses placed in an SEM. One of them is condenser lens, and the other one is an actual lens. These lenses coil electrons magnetically, which located below the electron gun. The electrons that focus with the help of lenses interact with the atoms in the sample.

The interaction between electrons and atoms produces three variety signals, which are X-rays, backscattered electrons, and secondary

electrons that can be detected through the detector. These detected signals give information about the surface topography.

The electron beam, which has a range of energy from ~ 100 eV to 100 keV is focused by two magnetic lenses into only one beam with a focal spot dimension from 1 nm to 5 nm [55]. The illustrated schema of SEM is shown in Fig. 3.11(a) [56]. Scanning electron microscopy is a non-destructive technique and it produces images which have very high-resolution. SEM can achieve a magnification from 10X to approximately 100,000X.

Scanning electron microscope Quanta FEG 250 (FEI®) which is shown in Fig. 3.11(b) equipped with EDS was used for the structural characterization of the sonochemically synthesized ZnO nanorods.

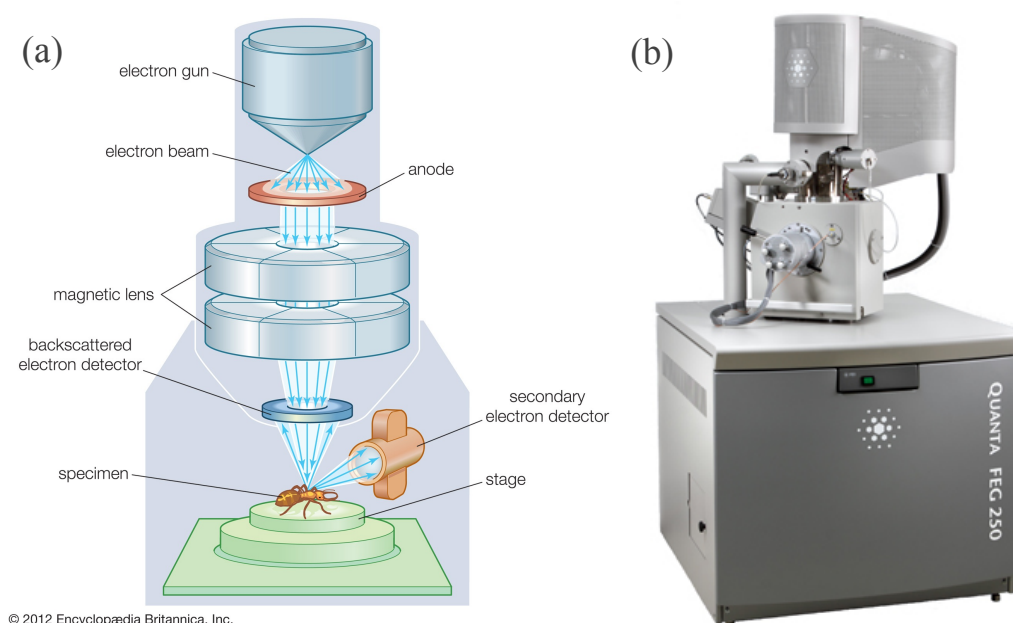


Figure 3.11 (a) Schematic working presentation of a SEM instrument, (b) The SEM instrument used for the characterization of ZnO nanorods.

3.2.3. Energy Dispersive X-ray Spectroscopy (EDS)

Energy Dispersive X-ray Spectroscopy (EDS, EDX or XEDS) is an X-ray microanalytical technique. Once the electron beam focuses on the substrate and penetrates through the sample, these electrons interact with atoms of the sample. It generates two types of X-rays; Bremsstrahlung X-rays and Characteristic X-rays. Bremsstrahlung X-rays mean braking radiation and also called as continuum or background X-rays.

When the ground-state electrons of the atom are under the electron beam, an electron from the inner shell excites and reaches to the higher energy-levels. It fills a hole in this level and leaves a hole behind. The energy difference between the higher-energy levels and the lower energy levels is released as X-rays. The sample emits these X-rays, and the number of emitted X-rays is reflected to the detector. Every element has its own peak in the X-ray spectrum, and these detected peaks are measured in the system as EDS. The X-rays in the EDS is shown in Fig. 3.12 [57].

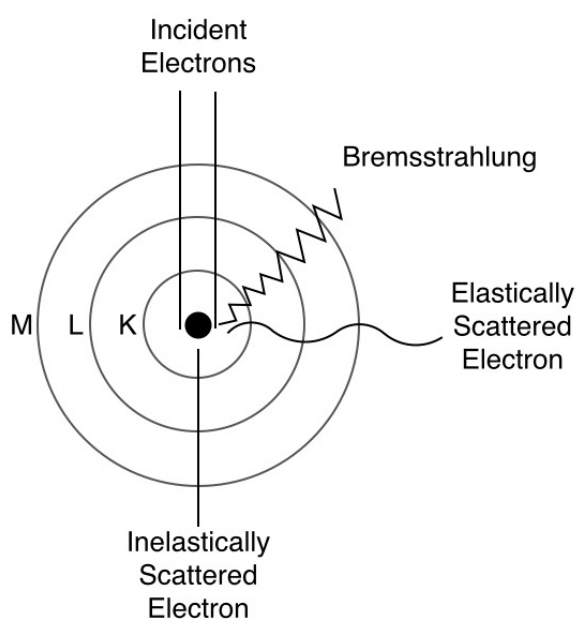


Figure 3.12 Working principle of EDS.

3.2.4. Raman Spectroscopy

Raman spectroscopy is a technique that is used to observe vibrational and other low-frequency modes in materials. In a Raman Spectroscopy, a sample is illuminated with a laser which can be in the visible, near infrared, or near ultraviolet range. Raman spectroscopy is a kind of vibrational spectroscopy, and it is much like infrared (IR) spectroscopy. However, IR depends on the change in the dipole moment of a molecule, while, Raman depends on the change in the polarizability. The working principle of Raman spectroscopy system is explained as, the laser from the illuminated spot is collected with a lens and sent through a monochromator. The wavelengths close to the laser line are filtered out, by the rules of Rayleigh Scattering, while the rest of the collected light is dispersed through the detector.

The Raman Effect occurs when the laser is impinged upon a sample, laser beam reaches to the molecule and reacts with the electrons and the bonds of that molecule and the photons of this molecule scatters. The majority of these scattered photons has the same wavelength of the incident photons and this is known as Rayleigh Scattering, a tiny portion (~ 1 in 10^7) of this scattered radiation shifts to a different wavelength. These shifted photons are called Raman Scattering. When the Raman scattered photons are shifted to further wavelengths, it is called as Stokes Raman Scattering. However, when a small portion is shifted to lowering wavelengths, it is called as Anti-Stokes Raman Scattering [55]. In each case, molecules are excited towards virtual state and then relaxed towards the ground state. The diagram of Rayleigh scattering, Stokes Raman scattering, and anti-Stokes Raman scattering is shown in Fig. 3.13.

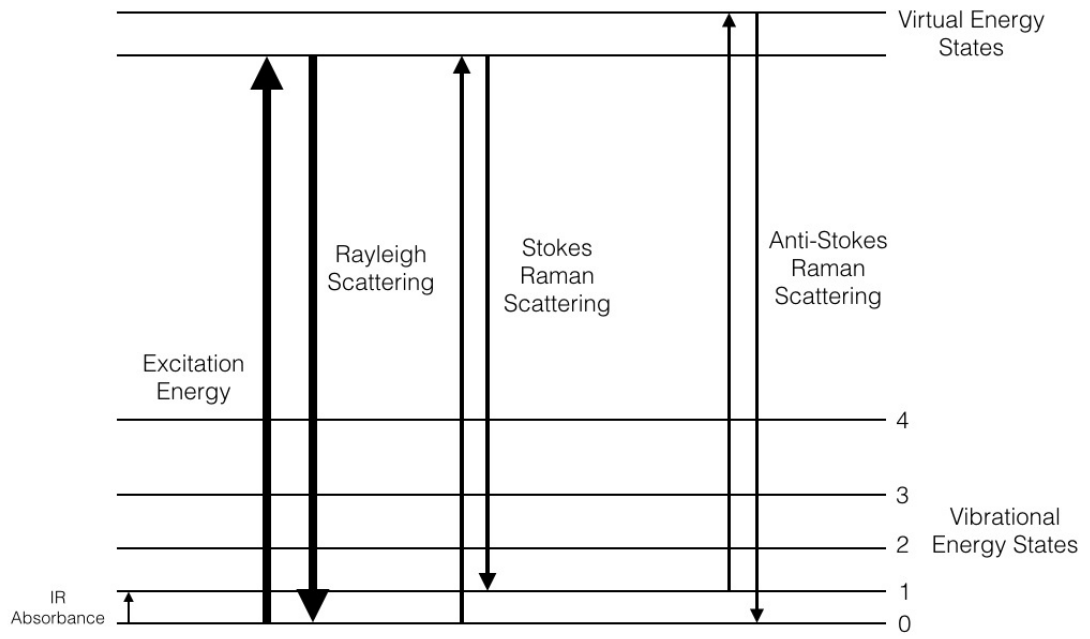


Figure 3.13 Energy level diagram of exciting states in the Raman effect.

4. RESULTS AND DISCUSSION

In this section, the characterization results of ZnO nanorods and their gas sensing responses under six different target gases, where five of them are toxic and four of them are VOC, are given. ZnO nanorods of various sizes were successfully synthesized on glass substrates by decomposition of zinc nitrate tetrahydrate and HMT at room temperature using sonochemistry. Growth was carried out within 30 - 60 min, subsequent to a 30 min seeding process as stated in the experimental section. Optical Microscope, Scanning Electron Microscope (SEM), Energy-dispersive X-ray spectroscopy (EDS), Raman Spectroscopy (RS) and Gas Absorption Measurement System used to analyze both the structural, elemental composition, and gas sensing properties of the sonochemically grown ZnO nanorods.

4.1. Morphological Characterization

Optical microscopy and scanning electron microscopy were used to examine the surface of the ZnO nanorods. These techniques give the information about the deposition of ZnO nanorods on the surface, and the structures obtained.

4.1.1. Optical Microscopy Analysis

The sample is characterized by an optic microscope. The optical microscope image of the gold (Au) electrodes is shown in Fig. 4.1. Zn based seed layer deposited on the glass substrate, prior to ZnO nanorod growth is shown in Fig. 4.2. The optical microscope images of ZnO nanorods are placed in Fig. 4.3. These images were taken from different points where the gold electrodes aren't deposited, at both low and high magnification.

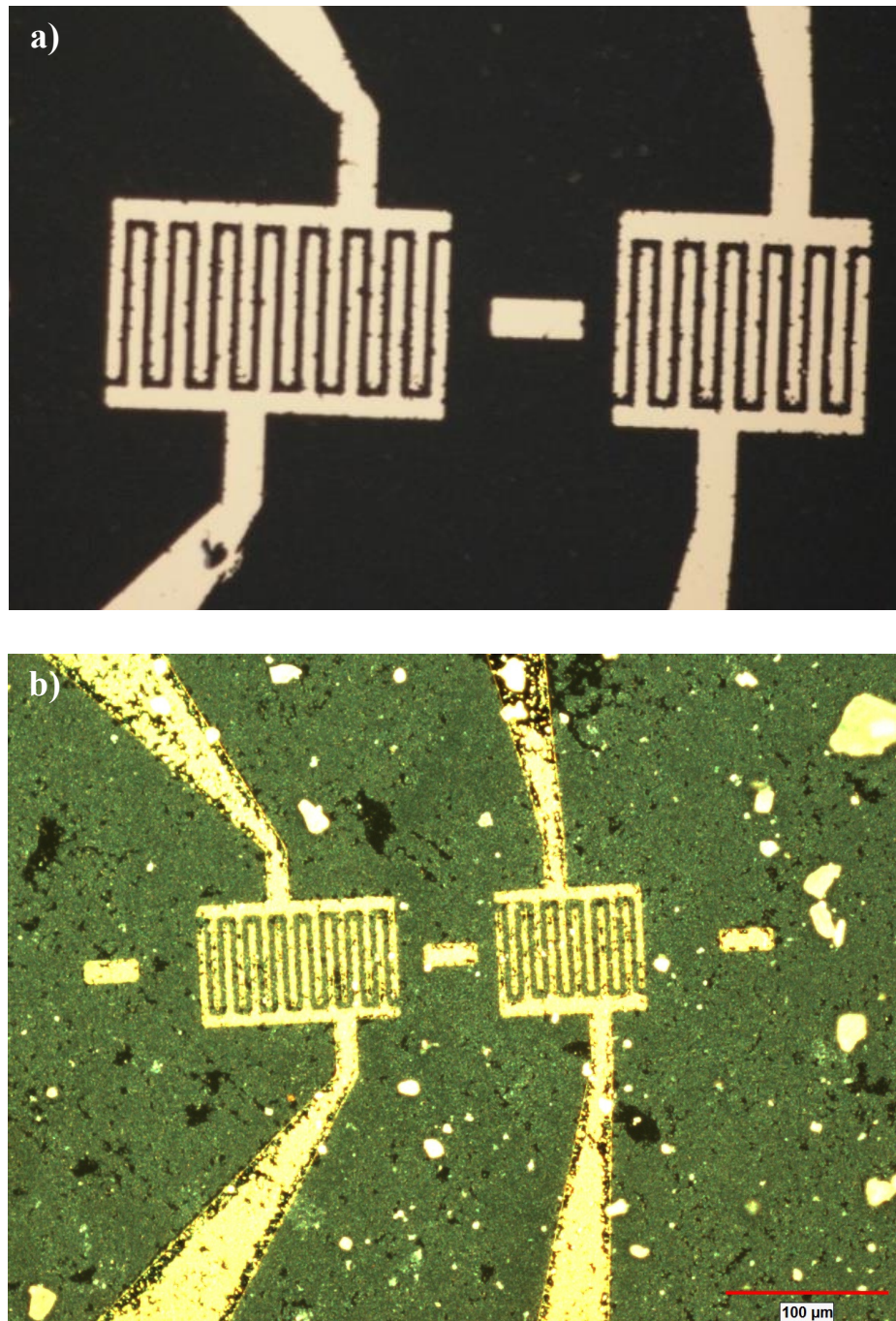


Figure 4.1 The image of IDE; (a) before the deposition ZnO nanorods, (b) after the deposition ZnO nanorods.

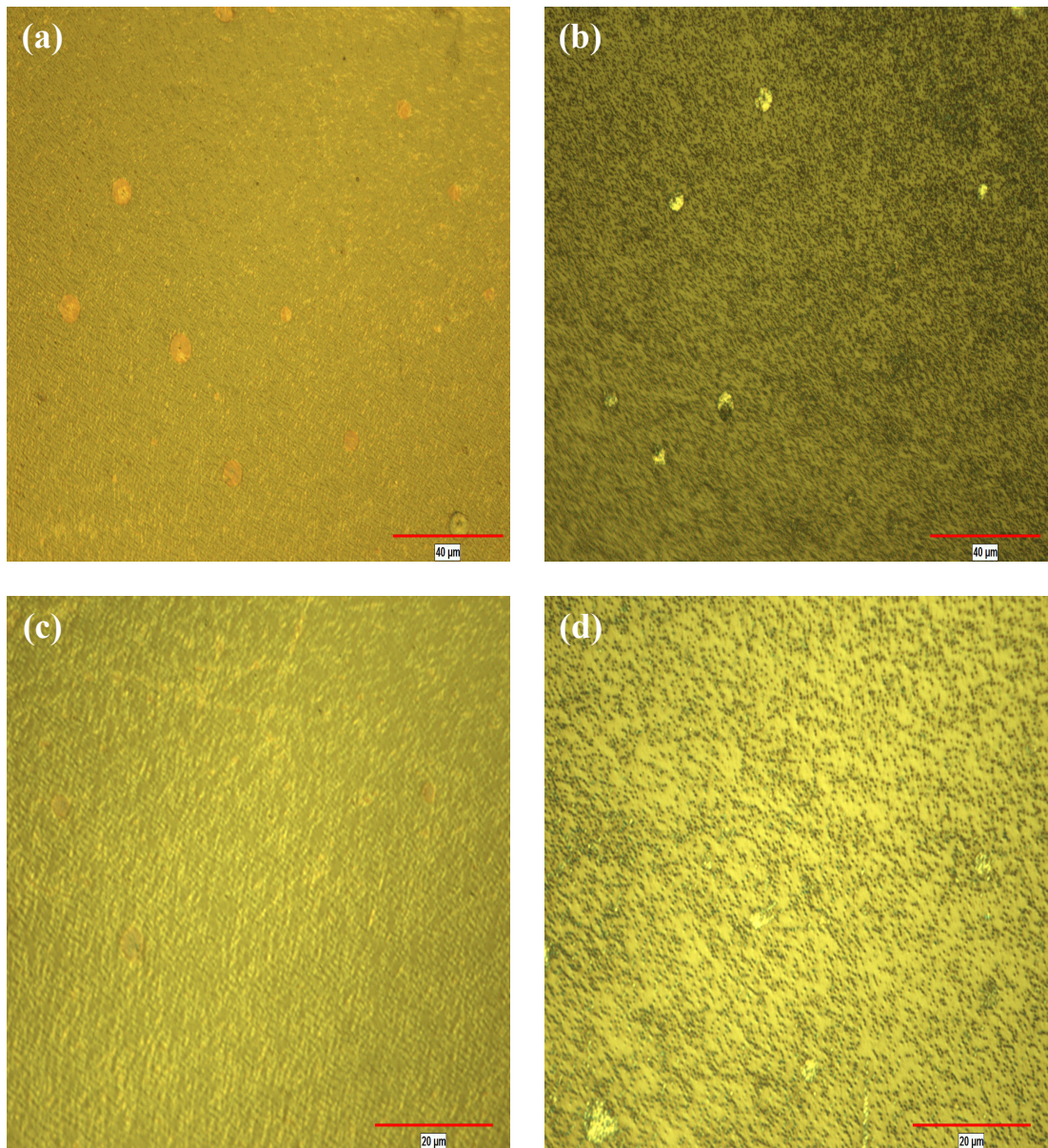


Figure 4.2 Optical microscope images of ZnO seed layer taken from 4 different areas; (a) and (b) areas are under low magnification (50x), (c) and (d) areas are under high magnification (100x).

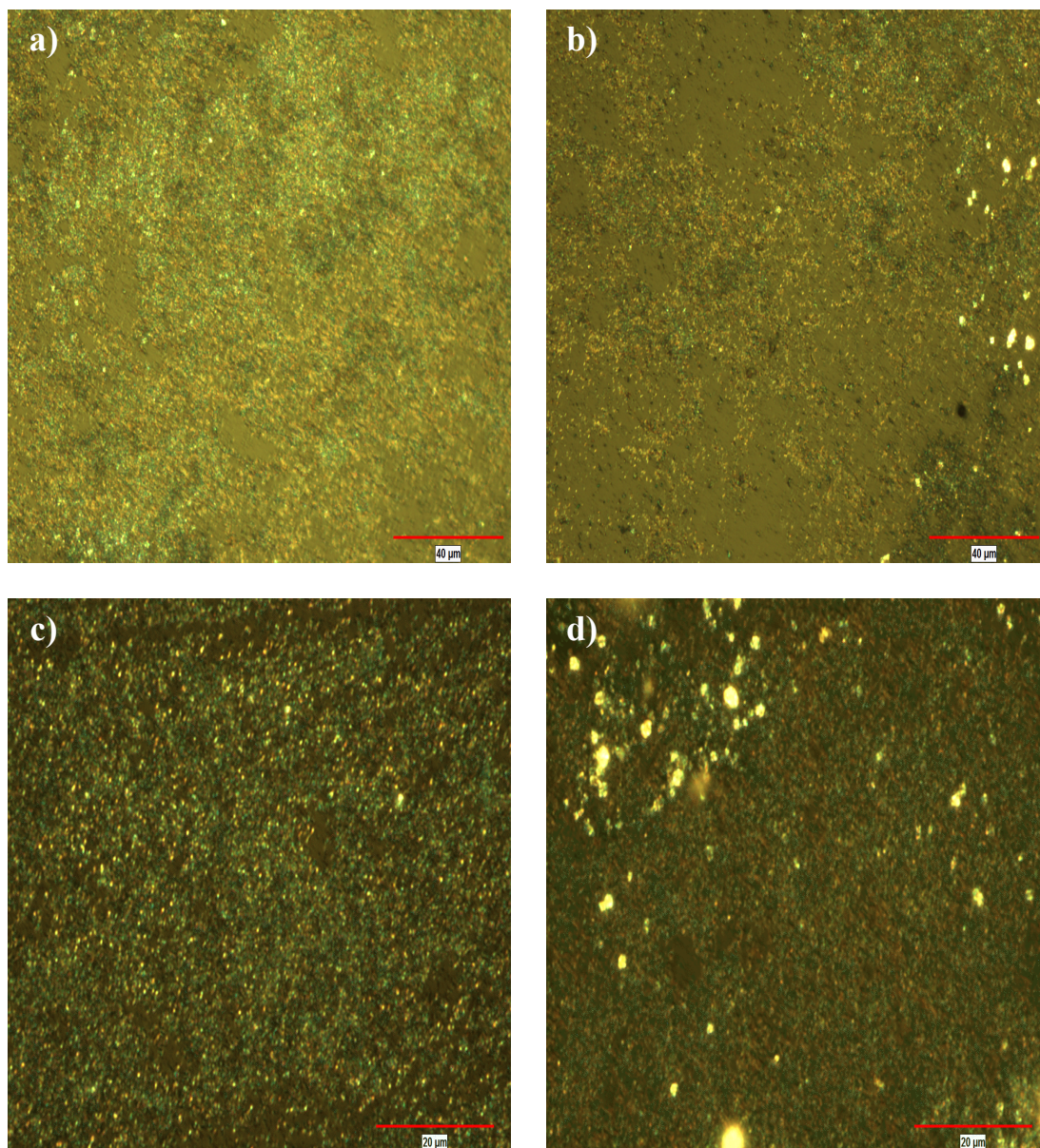


Figure 4.3 Optical microscope images of ZnO nanorod taken from different 4 areas; (a) and (b) areas are under low magnification (50x), (c) and (d) areas are under high magnification (100x).

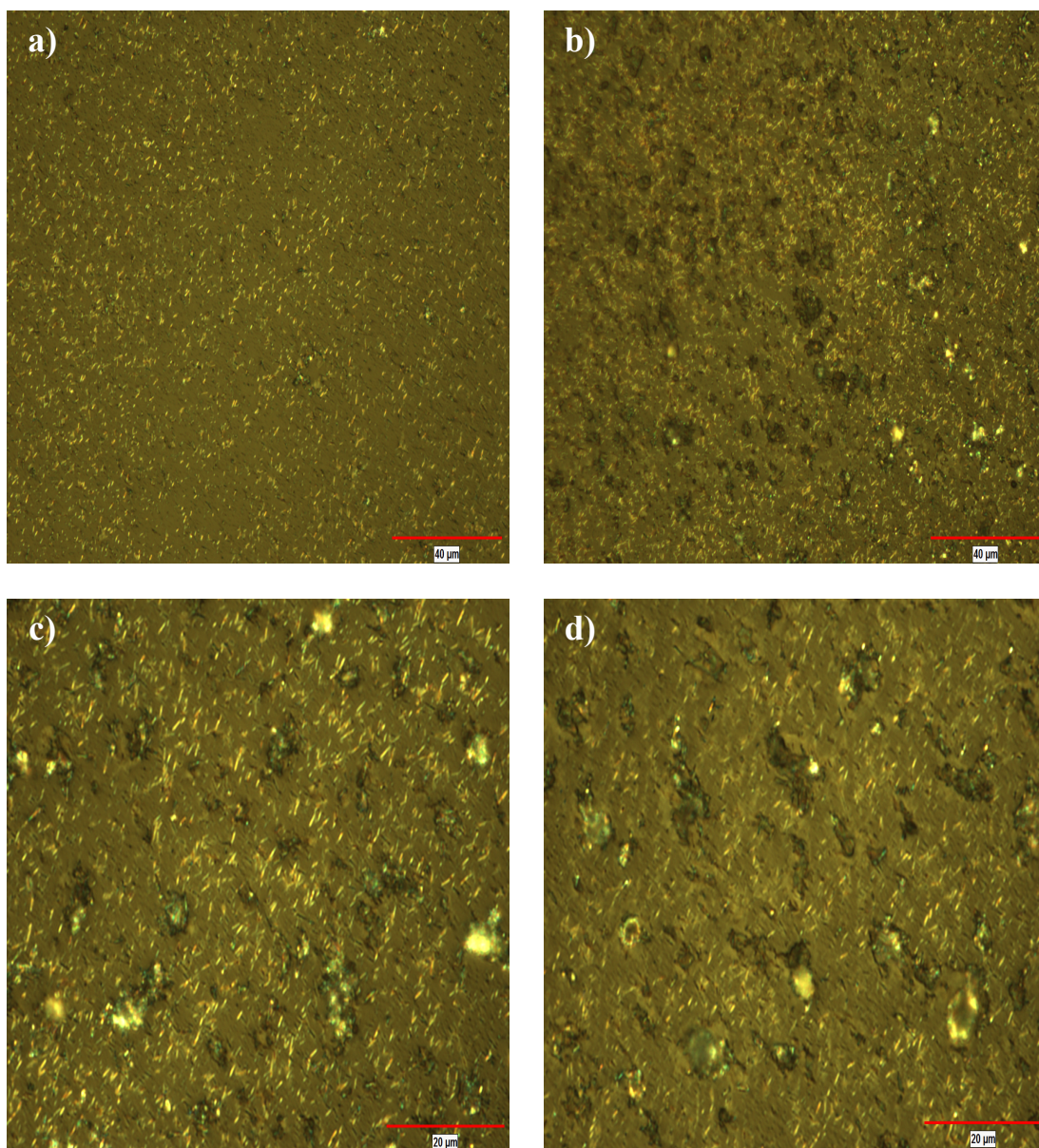


Figure 4.4 Optical microscope images of ZnO nanorod without seed layer of a trial sample taken from 4 different areas; (a) and (b) areas are under low magnification (50x), (c) and (d) areas are under high magnification (100x).

Low magnification images show the uniform distribution of ZnO nanoparticles on the glass substrate. In Figure 4.2 (a) and (b), which are ZnO seed layer covers the entire area. However, it's not homogenous. Zn particles congregate at some points. At these points, ZnO nanorod density is also increased. In the absence of the seed layer, ZnO nanorods are lying randomly on the substrate. This can be seen in the Fig. 4.4. In Figure 4.3, growth of the ZnO nanorods is not homogeneous, this supports the idea that ZnO nanorods grow denser where, the ZnO seedings accumulate. ZnO nanorods are grown as connected to each other. This creates a nanorod network for electrical conductivity.

4.1.2. Scanning Electron Microscopy Analysis

One of the morphological characterization tools for ZnO nanorods is Scanning Electron Microscopy (SEM). In some samples, SEM imaging can be problematic because of the conductivity. In order to obtain quality of SEM image, the samples may need to be coated with metallic layer depending on the material of the substrate. In this thesis, the sample wasn't coated with any metallic layer. The main reason is, if we coat our sample with any metallic layer, the gas sensing property of ZnO nanorods is meaningless. Electrons can be reflected to the detector via ZnO nanorods.

The Scanning Electron Microscope (SEM) images of the ZnO nanorods, grown by sonochemistry processes, were taken in the Izmir Institute of Technology - Center For Materials Research (IYTE-MAM). The images were taken in individual magnifications in 3 different areas. First, the SEM images of ZnO seed layer are placed in Fig. 4.5. Then, the images of ZnO nanorods are placed in the Fig. 4.6 and Fig. 4.7. EDS measurements were carried out after SEM images were taken in the same SEM.

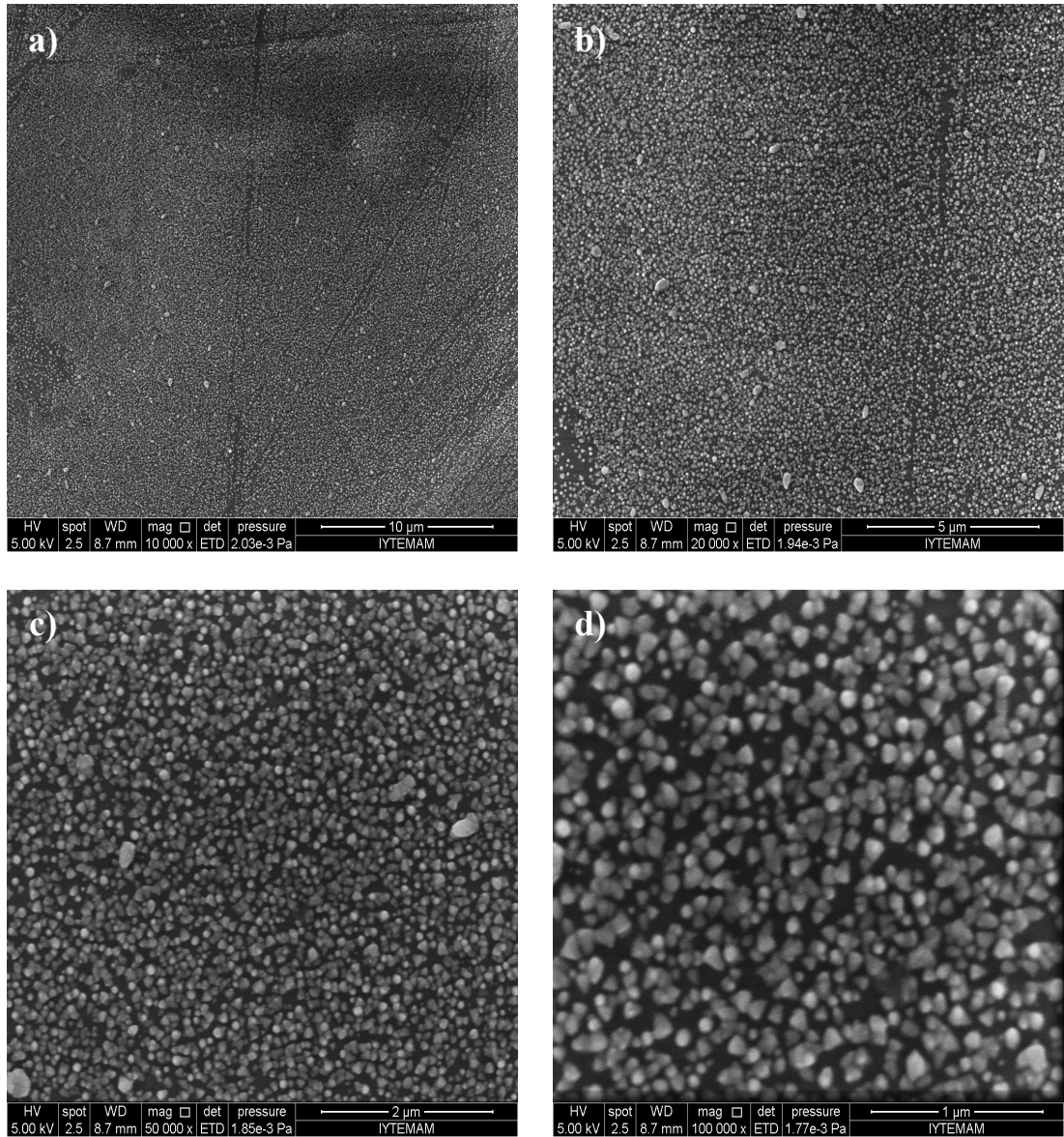


Figure 4.5 SEM images of ZnO seed layer; (a) and (b) are low magnifications (10000x-20000x respectively), (c) and (d) are high magnifications (50000x-100000x respectively).

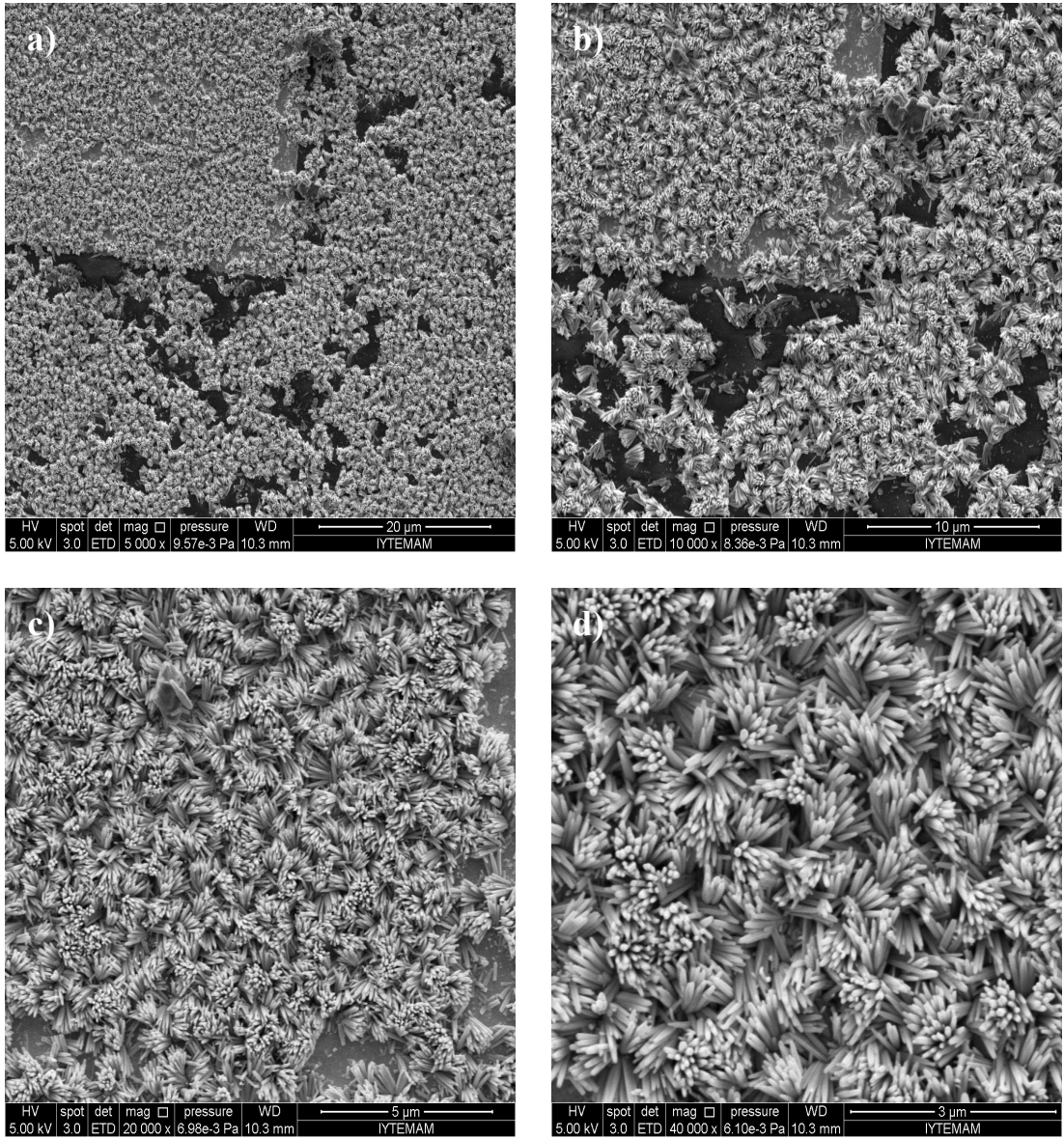


Figure 4.6 SEM images of ZnO nanorods; (a) and (b) are low magnifications (5000x-10000x respectively), (c) and (d) are high magnifications (20000x-40000x respectively).

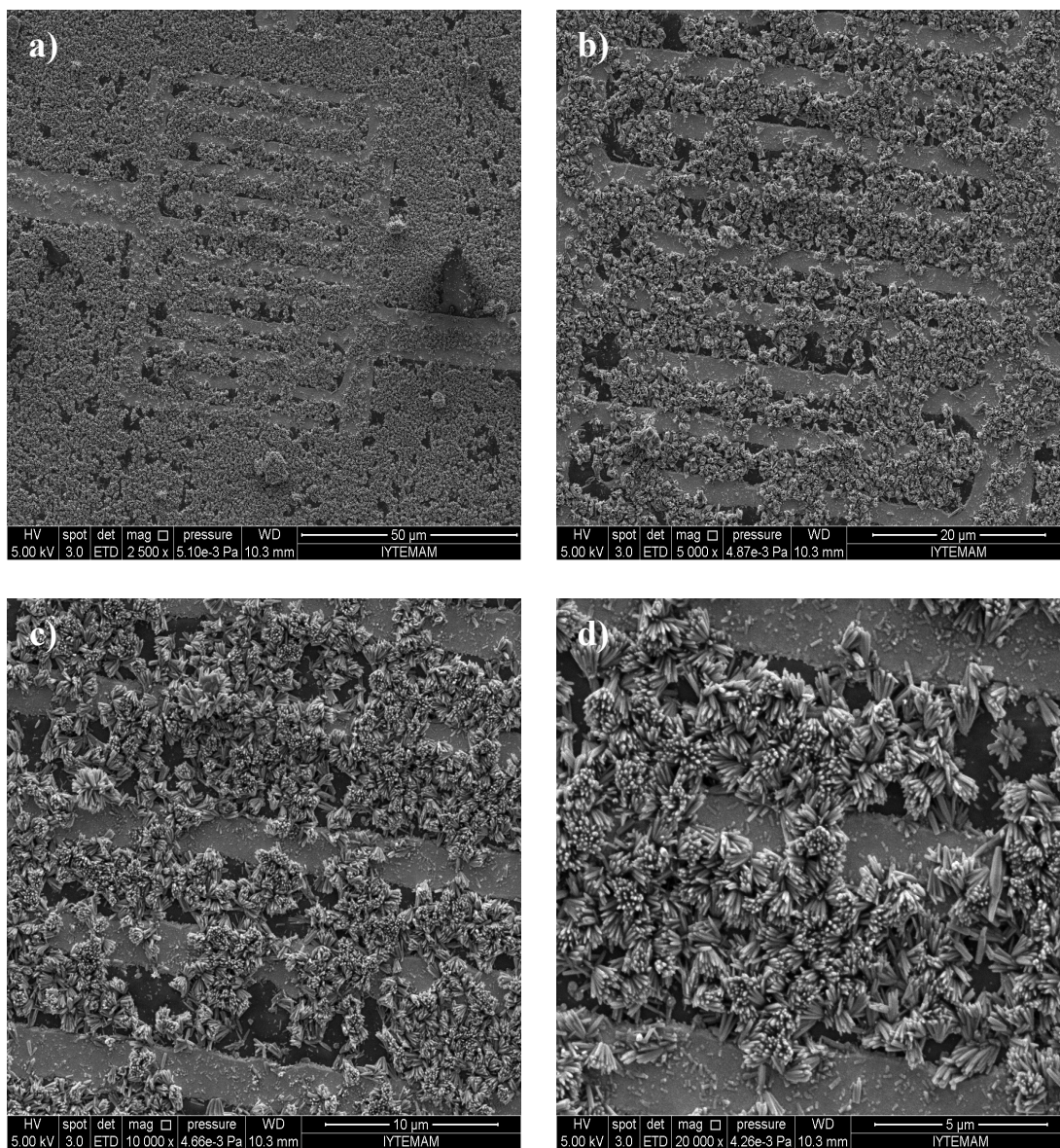


Figure 4.7 SEM images of ZnO nanorods on IDE electrodes; (a) and (b) are low magnifications (2500x-5000x respectively), (c) and (d) are high magnifications (10000x-20000x respectively).

Optical microscope images are in consistent with the SEM images. SEM images prove that the ZnO nanorods grown on the glass substrate are densely populated. As it was mentioned in the discussion of the optical microscopy images, ZnO nanorods coalesce at different locations on the substrate where ZnO particles of seed layer accumulate.

Sonication time is the most important parameter on the sonochemically grown ZnO nanorods. ZnO nanorods first were grown less densely with fewer aspect ratio for 30 min sonication. Then, sonication time was adjusted to 60 min from 30 min. This change resulted in more densely, populated and longer ZnO nanorods. The length of ZnO nanorods was ~450 nm and the diameter of ZnO was ~100 nm.

The surface morphology of the ZnO structures is in rod-like and hexagonal shape. However, some are observed to have been tapering and the sharp tips in the sensor. Furthermore, some ZnO nanorods tend to cluster and form a flower-like structure during the long sonication period as depicted in images.

As it can be seen from SEM the images, the whole surface is covered with some blank spots. However, the gaps between the IDE are covered with ZnO nanorod network. All the nanorods are in contact with each other and the gold electrodes. Therefore, they are creating a nanorod network.

4.2. Elemental Analysis

Elemental analysis of sonochemically grown ZnO nanorods was performed by Energy Dispersive X-ray Spectroscopy (EDS) and Raman spectroscopy.

4.2.1. Energy Dispersive X-ray Spectroscopy (EDS)

The composition of the ZnO nanorod was analyzed by energy dispersive spectroscopy (EDS). EDS map of ZnO nanorods is shown in Fig. 4.8 and the SEM image of the Spectrum 1 is shown in the Fig. 4.9. The major components of the ZnO nanorod based gas sensor are zinc, oxygen and gold. Zn has the highest amount in the EDS map, next gold, and then oxygen. The silicon (Si), carbon (C) and calcium (Ca) should be coming from the glass substrate.

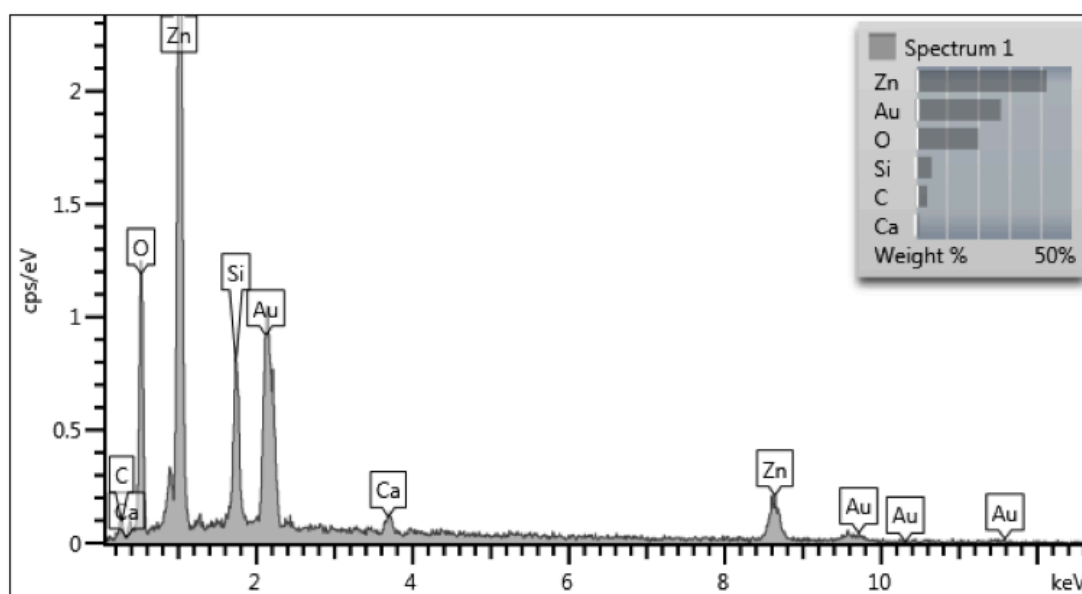


Figure 4.8 EDS spectrum of ZnO nanorod gas sensor.

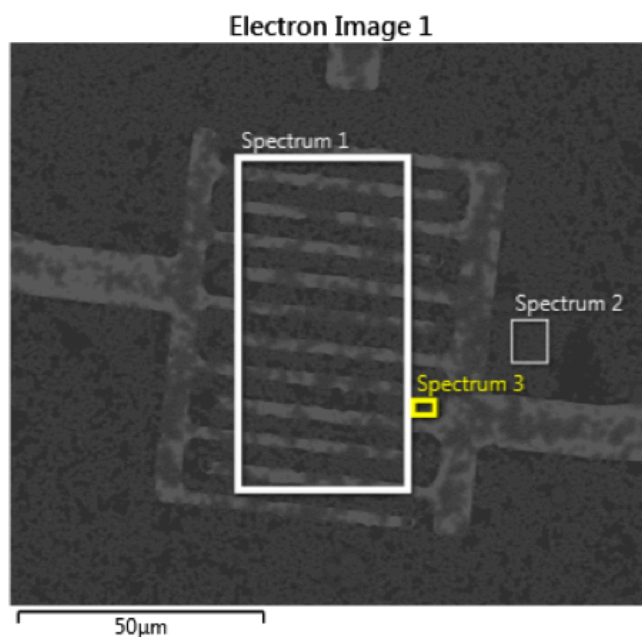


Figure 4.9 SEM image of EDS spectrums.

4.2.2. Raman Spectroscopy

Every material has its own characteristics in the Raman spectrum, which is considered as its finger print. Raman spectra is very sensitive to crystal quality, structural defect and the disorder of the particles. Therefore, Raman spectroscopy provides information about the structure of the particles. In this thesis, the wavelength of operating laser in Raman Spectroscopy is 488 nm.

The hexagonal wurtzite structure of ZnO belongs to the $C_4^6 V$ with two units per primitive cell. The Raman active optical phonon mode is $A_1 + 2E_2 + E_1$ which is predicted by group theory. A_1 and E_1 are the polar phonons which can split into transverse optical (TO) and longitudinal optical (LO) modes. E_2 is the non-polar mode which is composed of two modes frequency $E_{2(\text{high})}$ associated with vibration of the oxygen atoms and $E_{2(\text{low})}$ associated with vibration of the Zn sub-lattice.

The Raman measurement was performed in two different spots of the sample. $E_{2(\text{high})}$ mode is observed in all the spots, which is a finger print of ZnO wurtzite structure. In the Raman spectrum, there are many small peaks, the reason of these peaks is ZnO nanostructure presents incompatible characteristics compared to the bulk structure, and the divergence observed in the peak intensity can be explained as the different amount and unlike orientation of ZnO nanorods.

The peak at 97 cm^{-1} is assigned as the $E_{2(\text{low})}$ vibrational mode. $E_{2(\text{low})}$ peak shifted from the bulk value by $\sim 5\text{ cm}^{-1}$ which is due to the optical phonon confinement effect observes in nanostructures. The peak at 453 cm^{-1} is assigned as the $E_{2(\text{high})}$ which is shifted by a value of $\sim 16\text{ cm}^{-1}$. There is huge difference between the $E_{2(\text{low})}$ and $E_{2(\text{high})}$. The reason of this difference is O molecules are bigger than the Zn molecules. So, the vibration of O molecules are less than the Zn molecules under the wavelength of laser. The Raman spectra of the sonochemically grown ZnO nanorods is shown in Fig. 4.10.

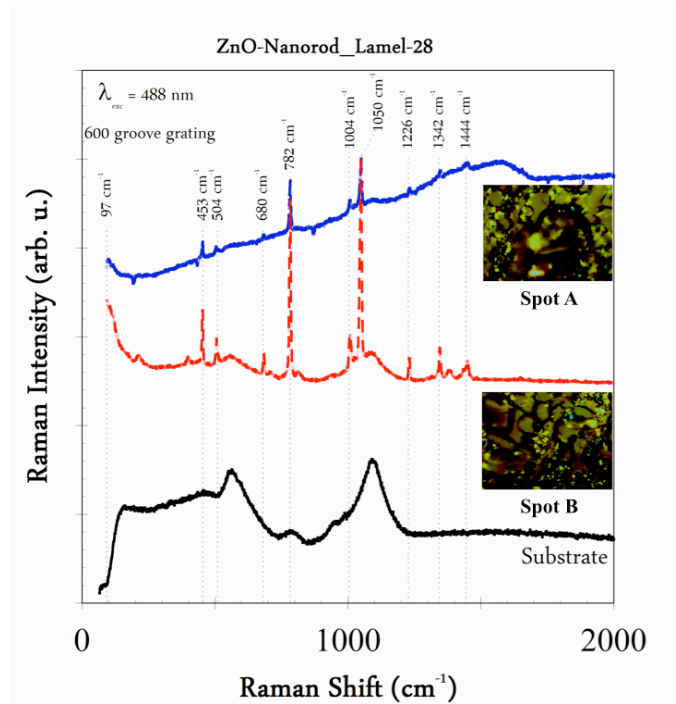


Figure 4.10 Raman spectrum of ZnO nanorod grown on glass substrate.

4.3. Gas Absorption Analysis

In this section, conductivity analyses based on gas sensing properties of sonochemically grown ZnO nanorods are presented according to the resistance change under the oxygen (O₂), carbon dioxide (CO₂), carbon monoxide (CO), ethanol (C₂H₅OH), isopropyl alcohol (C₃H₇OH), chloroform (CHCl₃) and dichloromethane (CH₂Cl₂) gases. Nitrogen (N₂) gas is used for desorption of targeted gasses.

The gas adsorption mechanism is shown in Fig. 4.11. When a target gas molecule is adsorbed on the surface of the ZnO nanorods, it produces an electrical response (the changing in resistance). The change in the resistance can be detected through an electrical measurement processor. In the measurement setup, which was used in the measurements of ZnO nanorod gas sensor MKS 647C Mass Flow and Pressure Programmer, MKS 179A Mass-Flo® mass flows and Keithley 2420 Source-meter were utilized.

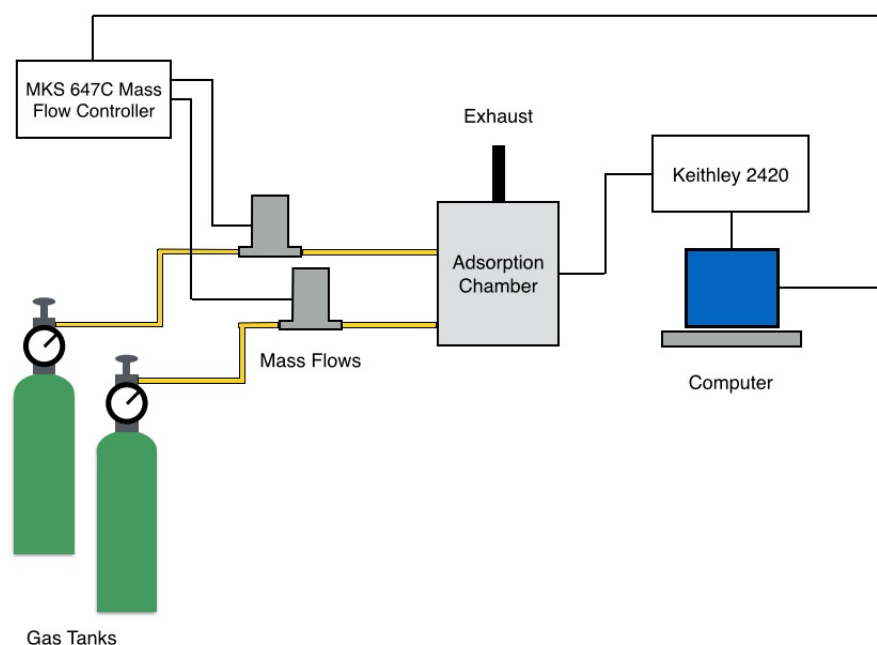
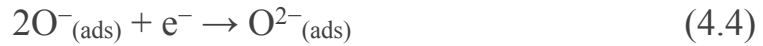
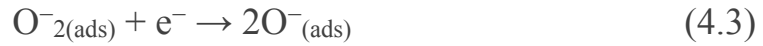


Figure 4.11 Schematic diagram of gas measurement system.

4.3.1. Oxygen (O₂) Response

Oxygen is one of the most active components of the air. There is approximately 20.9% oxygen by volume in the atmosphere. Therefore, we first consider ZnO surface exposed to normal air conditions. Oxygen vacancies on ZnO surfaces are electrically and chemically active. These vacancies, which act as donors, increase the surface conductivity.

When an oxygen molecule binds to the vacancies on the surface of the ZnO nanorods, they trap electrons from the surface of the ZnO. Then, ZnO nanorods remain tightly bounded as a charged oxygen anion. The trapped electrons of oxygen are resulted as increasing the resistance of the ZnO sensor. The oxidation process in ZnO nanorods occurs by the below states [58, 59];



In these reactions, $\text{O}^2_{(\text{gas})}$ and $\text{O}^2_{(\text{ads})}$ molecules are adsorbed on the surface respectively, e^{-} represents the electrons from ZnO. $\text{O}^{2-}_{(\text{ads})}$, $\text{O}^{-}_{(\text{ads})}$ and $\text{O}^{-}_{2(\text{ads})}$ represent the adsorbed surface oxygen species.

The measurement of O₂ was performed under high purified nitrogen at room temperature in a closed chamber. The measurement result is shown in Fig. 4.12. The targeted O₂ gas was carried out with a flow rate of 500 sccm for 1200 seconds and cleaned by N₂. The voltage applied to the sensor was 3 V. At the 0-200th, the sensor is under N₂ to clean the environment, to desorb the surface of ZnO nanorods from target gas. Afterwards, O₂ was pumped into the chamber between 200th-400th. Then, N₂ was flowed a second time and stop pumping N₂ until 600th to clean the chamber from O₂. O₂ was pumped into the

chamber after 600th once more until 800th. Nitrogen was pumped until 1000th one more time. Then, O₂ was pumped once again until 1200th. As It can be seen from the graph that, resistance is increasing under O₂ as it was mentioned in literature. Under N₂, resistance decreases. As it can be seen, the resistance of the sensor is also increasing in some points of N₂ after first loop. The reason for this might be, the chamber and the surface of the ZnO nanorods were not completely cleaned from the O₂.

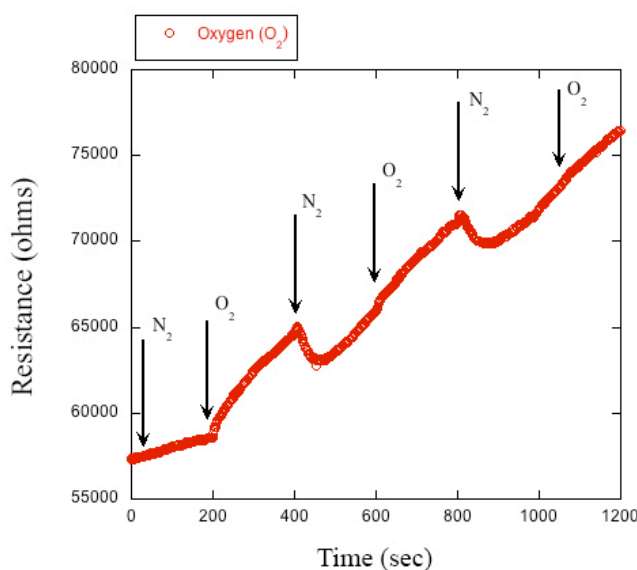


Figure 4.12 The Resistance (R) - Time (T) measurement of ZnO nanorod gas sensor under O₂.

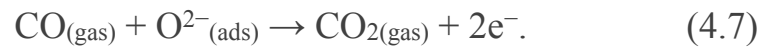
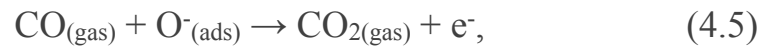
4.3.2. Carbon Monoxide (CO) Response

Carbon monoxide (CO) gas consists of one carbon atom and one oxygen atom, connected by a triple bond that consists of two and one dative covalent bonds. Carbon-containing compounds can produce CO by the partial oxidation. When there is not enough oxygen to produce carbon dioxide (CO₂) in the environment, CO starts to form. In the presence of oxygen, including atmospheric concentrations, carbon monoxide burns with a blue flame, producing carbon dioxide.

The molar mass of CO is 28.0 (g.mol⁻¹), which makes it slightly lighter than air, whose average molar mass is 28.8 (g.mol⁻¹). The bond

dissociation energy is 1072 (kJ/mol) and represents the strongest chemical bond as known. Carbon (C) and oxygen (O) atoms together have a total of 10 valence electrons (e^-) in carbon monoxide. Carbon and oxygen atoms in CO form triple bond with six shared electrons in three bonding molecular orbitals.

Carbon monoxide (CO) is a reducing gas. So, when it is in contact with the surface, they react with ionically adsorbed oxygen and release carbon dioxide (CO_2) to the air. Reaction states of oxidation are as follows [60];



During these states, the oxygen concentration of surface is reduced, and initially trapped electrons by oxygen anions are released back into the ZnO nanorods. Because of this, the conductivity of the sensor begins to increase as shown in the Fig. 4.13.

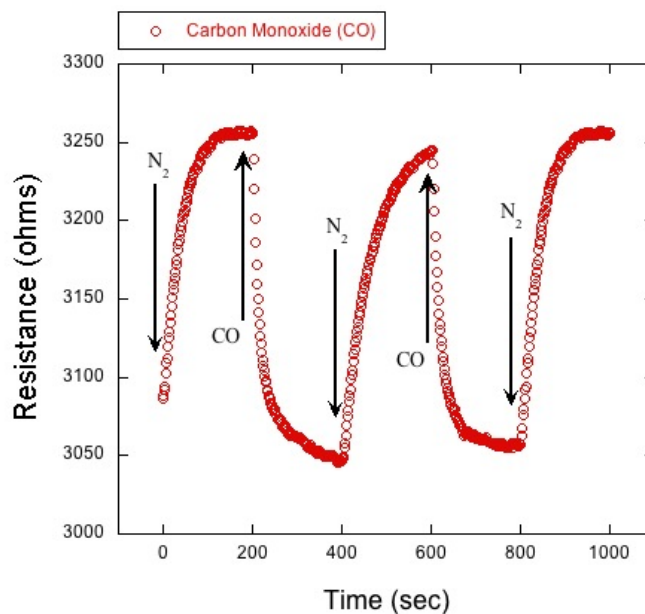


Figure 4.13 The Resistance (R) - Time (T) measurement of ZnO nanorod gas sensor under CO.

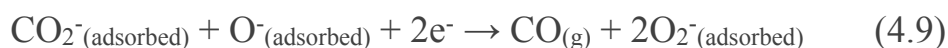
The adsorption of CO was measured at room temperature in a closed chamber. The targeted CO gas carried out with a flow rate of 500 sccm into the chamber. Purified N₂ gas was used to break CO molecules from the sensor. The voltage applied to the sensor was 10 V. Between 0-200th, the sensor is under N₂. Following, CO was pumped into the chamber in 200th-400th. Then, N₂ was streamed once again until 600th to clean the chamber from CO. CO was flowed into the chamber from 600th to 800th once more. N₂ was pumped until 1000th for the last time. As it can be seen from the graph that, resistance decreases under CO gas as it was mentioned in the literature while resistance increases under N₂ gas.

4.3.3. Carbon Dioxide (CO₂) Response

Carbon dioxide is a part of Earth's atmosphere, which covers 0,037 % of air. Carbon dioxide is a major part of greenhouse gases, and its emission increases day by day. Thus, detecting CO₂ concentration is very crucial in both indoor and outdoor environments.

CO₂ is formed by two O and single C atoms naturally. It has a sharp acidic odor at high concentrations. The density of CO₂ is around 1.98 kg/m³.

When ZnO nanorods of the sensor were exposed to CO₂ gas, CO₂ reacts with the adsorbed O⁻ and extracts the electrons from the conduction band of ZnO nanorods. The resistance change of ZnO gas sensor under CO₂ gas is shown in the Fig. 4.14. The possible reactions of CO₂ with O ion is given below [61, 62];



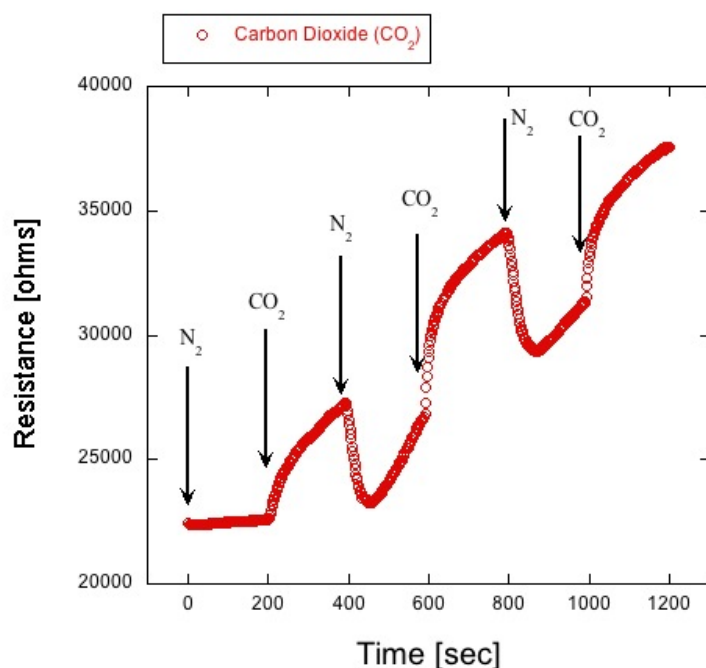


Figure 4.14 The Resistance (R) - Time (T) measurement of ZnO nanorod gas sensor under CO₂.

CO₂ sensor measurements were carried out in the room temperature. The targeted CO₂ gas was streamed with a flow rate of 500 sccm for 1200 seconds. The voltage applied to the sensor was 3 V. The sensor was under N₂, between the 0-200th. Ensuing, CO₂ was pumped into the chamber at 200th-400th. Then, N₂ was pumped again until 600th to clean the chamber from CO₂. CO₂ was pumped into the chamber after until 800th once again. N₂ gas was pumped until 1000th once more. Then, CO₂ gas was pumped until 1200th for the last time.

When the ZnO nanorod gas sensor is under CO₂ which is a reducing gas, resistance of the sensor increases as it was mentioned in the literature. The reason for the resistivity increase after N₂ pumping between the 400th-600th should be contributed non-complete cleaning of CO₂ from the sensor surface. The other reason could be that CO₂ adsorbs CO which increases the resistance. In the 600th and 1000th, when the CO₂ was pumped, the resistance started to increase immediately.

4.3.4. Ethanol (C₂H₅OH) Response

Ethanol is a volatile, flammable, colorless, slight odor liquid with the structural formula CH₃CH₂OH, often abbreviated as C₂H₅OH. Ethanol's hydroxyl group can participate in hydrogen bonding, rendering it more viscous and less evaporative than fewer polar organic compounds of similar molecular weight. Ethanol can be oxidized to acetaldehyde (CH₃CHO) (dehydrogenation) and ethylene (C₂H₄) (dehydration) [63]. These processes are illustrated in Fig. 4.15 [64]. However, the further oxidation goes to acetic acid, depending on the reagents and conditions [65, 66]. The oxidation states of ethanol to acetaldehyde and ethylene are;



The final state of oxidation of ethanol leads to CO₂ and H₂O, which the states are;

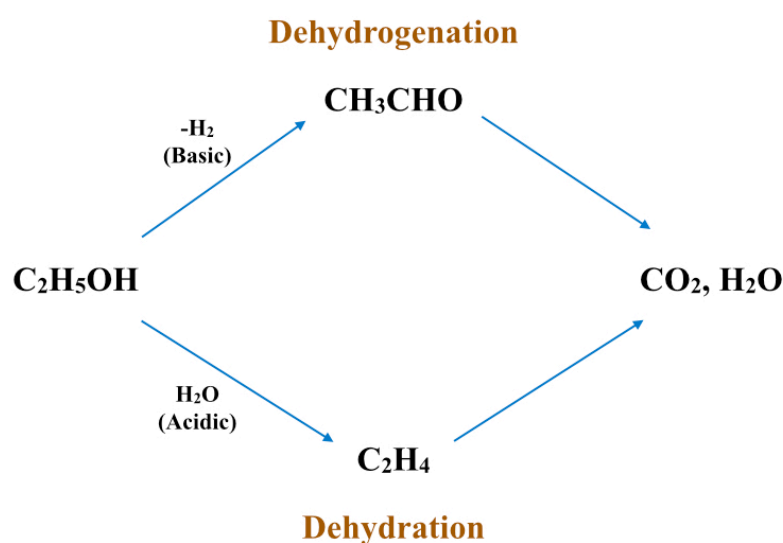
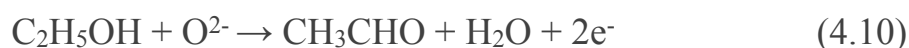


Figure 4.15 Routes of oxidation of ethanol vapor.

When the ZnO nanorod surface is exposed to ethanol vapor, the surface is chemisorbed with the ethanol gas and O^{2-} takes place. During chemisorption, electrons begin to be released into the depletion layer and electrical conductance of the ZnO nanorod sensor increases. The measurement of C_2H_5OH is given in the Fig. 4.16.

The adsorption of ethanol was measured at room temperature in a closed chamber. The targeted ethanol molecules were carried at a flow rate of 500 sccm for the total of 600 seconds via highly purified dry air from a bottle of ethanol liquid. The voltage applied to the sensor was 3 V. At the 0-200th, the sensor was under N_2 exposure. In the following, ethanol was pumped into the chamber at 200th-400th. Then, N_2 was pumped again until 600th to clean the chamber from ethanol. As It can be seen from the graph that, resistance decreases under ethanol since, resistance increases under N_2 as it was mentioned in the literature.

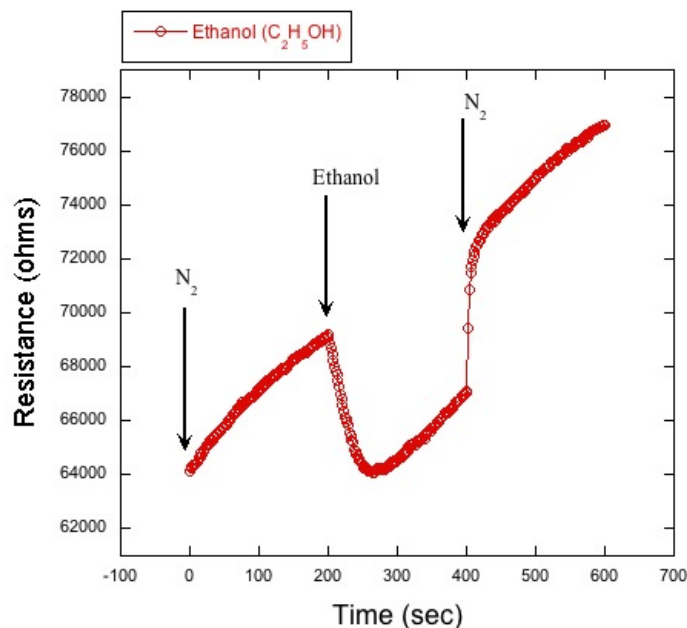


Figure 4.16 The Resistance (R) - Time (T) measurement of ZnO nanorod gas sensor under ethanol.

In this thesis, two types of measurement were performed for some target gases. These measurements are periodic and linear measurements.

The linear measurements were consistent with periodic measurements. The way of measuring the target gases linearly was concluded by accelerating the concentrations of target gases of 2% at every 5 seconds from 0% to 100%, when the concentration is reached to 100% in the chamber, concentration of gases was started to pump back until the concentration is 0%. In the Figure 4.17, the linear measurement had been implemented for 1480th seconds in three loops where the ethanol concentration reached to 0% at 3V with a flow rate of 500 sccm. At the 220th, the ethanol concentration is reached to 100% and pumped back to 0% at 520th. The other 100% concentrations are at 730th, 1240th and 0% concentrations are at 1020th, 1480th.

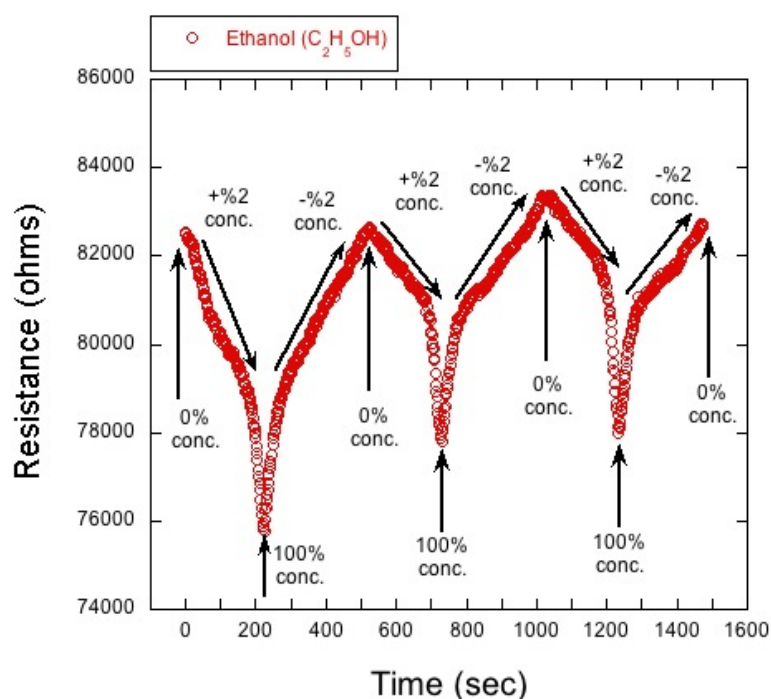


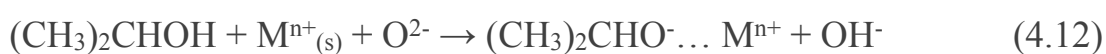
Figure 4.17 Linear measurement of ZnO nanorod gas sensor under ethanol.

4.3.5. Isopropyl Alcohol (C₃H₇OH) Response

The molecular formula of isopropyl alcohol (IPA) is (CH₃)₂CHOH. It appears as a clear, colorless liquid. It's the most common example of secondary alcohol and isomer of 1-propanol. The alcohol carbon atom of isopropyl alcohol is attached to two different

carbon atom. IPA is highly flammable. The vapor form of IPA can be explosive with air. Toxic gases which are carbon oxides (CO₂, CO) and hydrocarbons, can be released from IPA when heated.

IPA is a reducing gas. Therefore, when ZnO nanorods were exposed to IPA with the adsorbed oxygen on the surface of nanorods, ZnO receives electrons from IPA, and the resistance is reduced. IPA oxidizes to acetone and propylene and oxidation states of IPA is given below [67, 68];



Mⁿ⁺ is the positive metal cation to which the surface isopropoxide species are bonded. The adsorption measurement of C₃H₇OH is given in the Fig. 4.18.

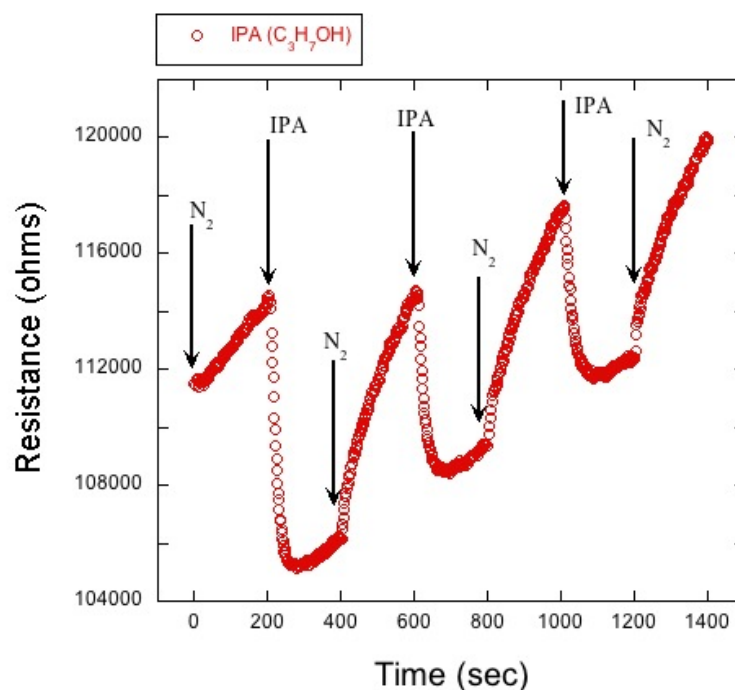


Figure 4.18 The Resistance (R) -Time (T) measurement of ZnO nanorod gas sensor under IPA.

The adsorption of IPA was measured at room temperature in a closed chamber. The targeted IPA molecules were streamed at a flow rate of 500 sccm for 1600 seconds via highly purified dry air from a bottle of IPA liquid. The voltage which applied to the sensor was 3 V. At the 0-200th, the sensor was under N₂. After that, IPA was pumped into the chamber at 200th-400th. Then, N₂ was pumped again until 600th to clean the chamber from IPA. This process performed in three loops. As it can be seen from the graph that, resistance decreases under IPA gas as it was mentioned in the literature.

Additionally, the linear measurement of IPA is consistent with periodic measurement of IPA and given in the Fig. 4.19. The concentration of IPA is increased by 2% at every 5 seconds from 0% to 100%, and pump backward until the concentration reached to 0%. The linear measurement was carried out for 500 at 3V with a flow rate of 500 sccm. At the 210th, the IPA concentration is reached to 100% and pumped back to 0% at 500th.

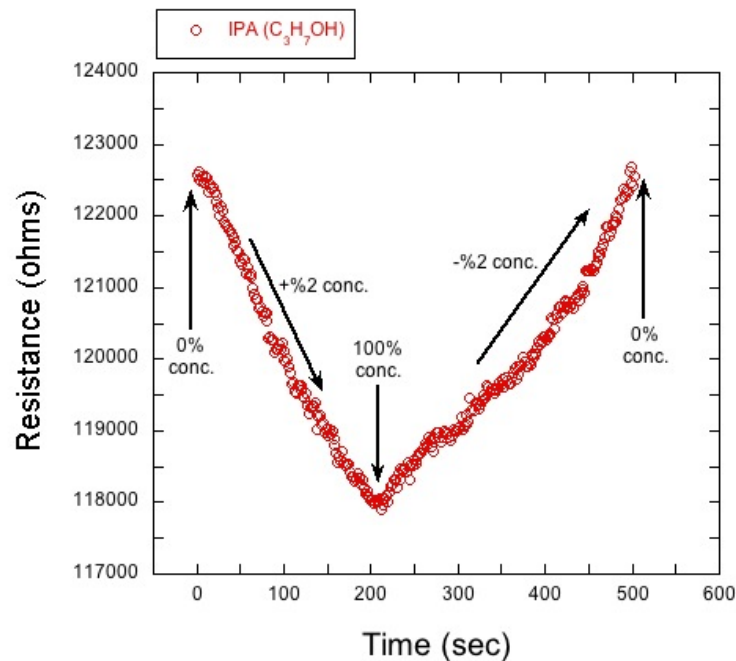


Figure 4.19 Linear measurement of ZnO nanorod gas sensor under IPA.

4.3.6. Chloroform (CHCl₃) Response

Chloroform is an organic compound which is one of the four chloromethanes. It is colorless, sweet-smelling, in dense liquid form and considered as toxic. The natural sources of chloroform are both biogenic and abiotic and 90% of atmospheric chloroform comes from these sources. Chloroform is widely used in medical surgeries for anesthesia because of suppressing effect of the central nervous system, in the pharmaceutical industry as sedative.

Chloroform is also a reducing gas which decreases the resistance of ZnO nanorods when exposed. The adsorption of reducing gases on ZnO nanorods was explained in previous sections. The oxidation state of chloroform is given below [69] and chloroform measurement is given in the Fig. 4.20;

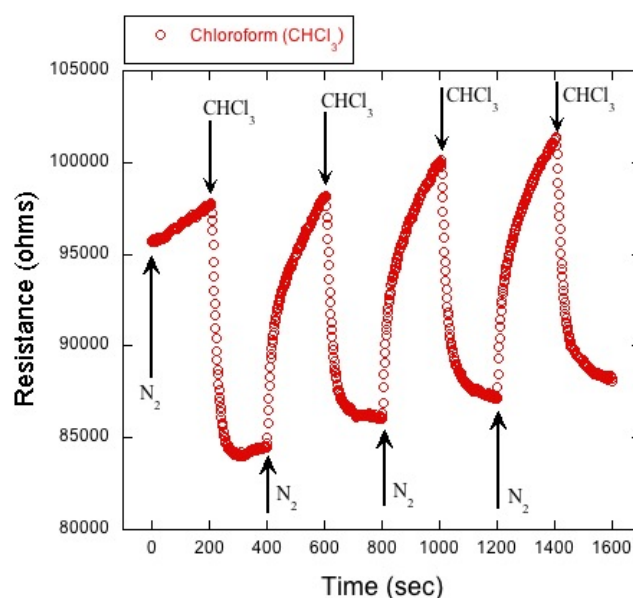
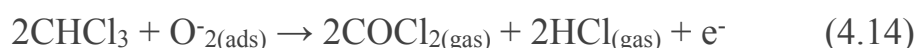


Figure 4.20 The Resistance (R) - Time (T) measurement of ZnO nanorod gas sensor under chloroform.

The targeted chloroform molecules were carried to the chamber with a flow rate of 500 sccm for 1500 seconds via highly purified dry air

from a bottle of liquid chloroform. The voltage applied to the sensor was 3 V. At the 0-200th, the sensor is under N₂. Afterwards, chloroform was pumped into the chamber between 200th-400th. Then, N₂ was pumped again until 600th to clean the chamber from chloroform. As it can be seen from the graph that, resistance decreases under chloroform gas as it was pointed out in the literature.

The linear measurement of chloroform is consistent with periodic measurement of chloroform like the previous results, and given in the Fig. 4.21. The result is completed similar to those measurements as it was applied. The linear measurement was operated for 1500 seconds at 3V at a flow rate of 500 sccm. At the 250th, the chloroform concentration was reached to 100% and pumped back to 0% at 515th. At the second loop, the concentration is reached to 100% percent at 750th and pumped backward to 0% at 1030th. At the third loop, the concentration is reached to 100% percent at 1260th and pumped back to 0% at 1500th.

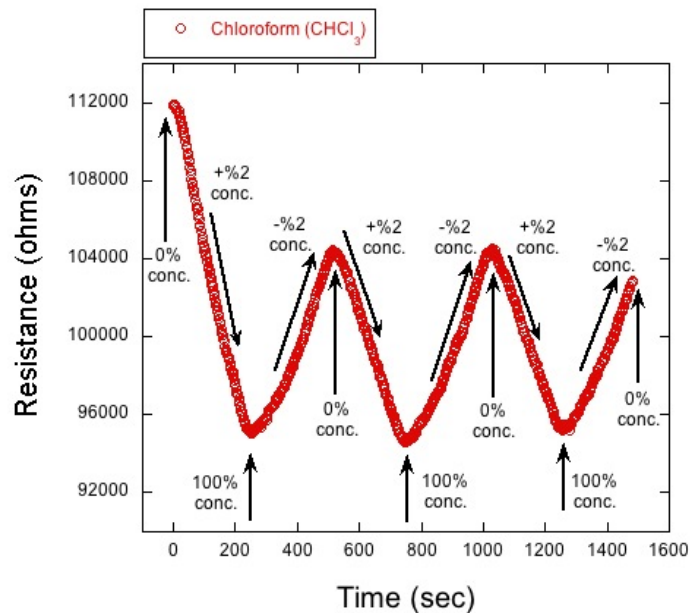


Figure 4.21 Linear measurement of ZnO nanorod gas sensor under chloroform.

4.3.7. Dichloromethane (CH₂Cl₂) Response

Dichloromethane (DCM) is a kind of organic compound, which is a halogenated aliphatic hydrocarbon compound. It is colorless and has a sweet odor. Vapor form of DCM is heavier than the air. It is stable, incombustible and non-explosive when mixed with air below 100 °C. The bonds of DCM occur as C–H and C–Cl by a single atom. The natural sources of DCM are oceanic assets, macroalgae, wetlands, and volcanoes. The majority source of DCM is industrial emissions. Humans may be exposed to DCM through air, drinking water, food and soil, and the absorption of DCM occurs rapidly in the body.

DCM is also a reducing gas which reacts with O⁻ ions and decreases the resistance of ZnO nanorods [70, 71]. The oxidation state of DCM is given below [72] and DCM measurement is given in Fig. 4.22;

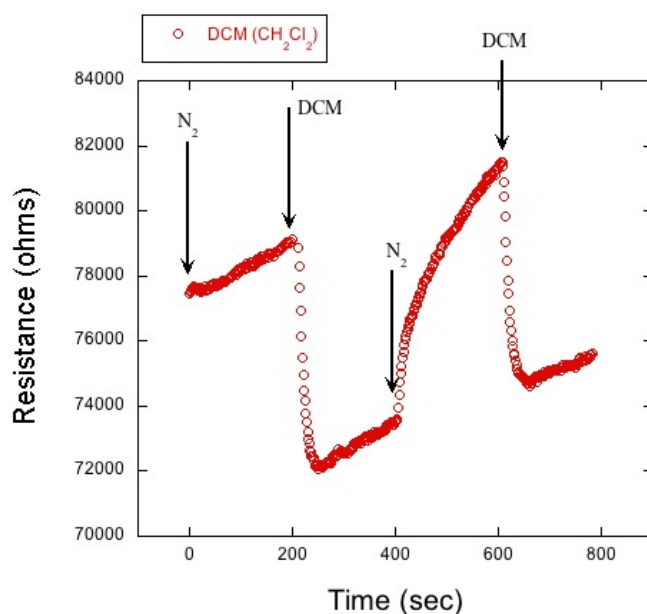


Figure 4.22 The Resistance (R) -Time (T) measurement of ZnO nanorod gas sensor under DCM.

The targeted DCM molecules were carried out with a flow rate of 500 sccm for 800 seconds via highly purified dry air from a bottle of

DCM liquid. Applied voltage to the sensor was 3 V. The sensor is under N_2 at the 0-200th. Later, DCM was pumped into the chamber between 200-400 seconds. Then, N_2 gas was pumped again until 600th to clean the chamber from DCM. After that, DCM was pumped into the chamber between 800th-600th once again. As It can be seen from the graph that, resistance of the sensor decreases under DCM and resistance increases under N_2 as it was pointed out in the literature.

The linear measurement of DCM is also consistent with periodic measurement of DCM in addition to previous results, and given in the Fig. 4.23. The measurement was carried out for 1500 seconds at 3 V with a flow rate of 500 sccm in the same way as it was mentioned. At the 220th, the concentration of DCM reached to 100% and pumped back to 0% at 510th. At the second loop, the concentration is reached to 100% percent at 725th and pumped backward to 0% at 1020th. At the third loop, the concentration reached to 100% percent at 1230th and pumped down to 0% at 1480th.

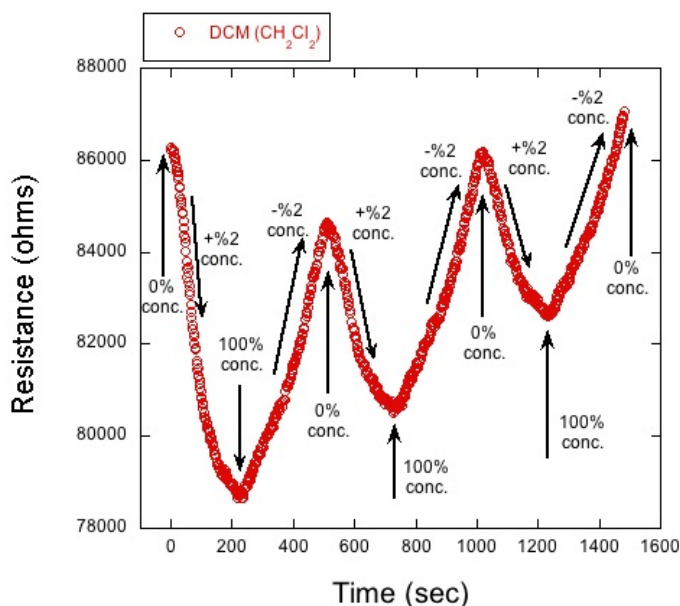


Figure 4.23 Linear measurement of ZnO nanorod gas sensor under DCM.

All the target gas results are given individually, so that the sensitivity values of the sensor to each gas can be compared. Sensitivity values are calculated by the formula of;

$$(S \%) = ((R_{\text{air}} - R_{\text{gas}}) / R_{\text{air}}] \times 100 \quad (4.16)$$

If we consider the sensitivity values in Fig. 4.24, prepared ZnO nanorods confirmed very good response. The figure shows that the sensor is the most sensitive to chloroform compared to other target gases. This can be explained as, the adsorption of chloroform is very high on the ZnO nanorods compared to others. However, the sensitivity of sensor for CO₂, ethanol, IPA and DCM was close to chloroform. As it was mentioned in the oxygen response part, the resistance change in the sensor for O₂ were not as big as others. Therefore, the sensitivity of the sensor to oxygen gas is low compared to the other target gases.

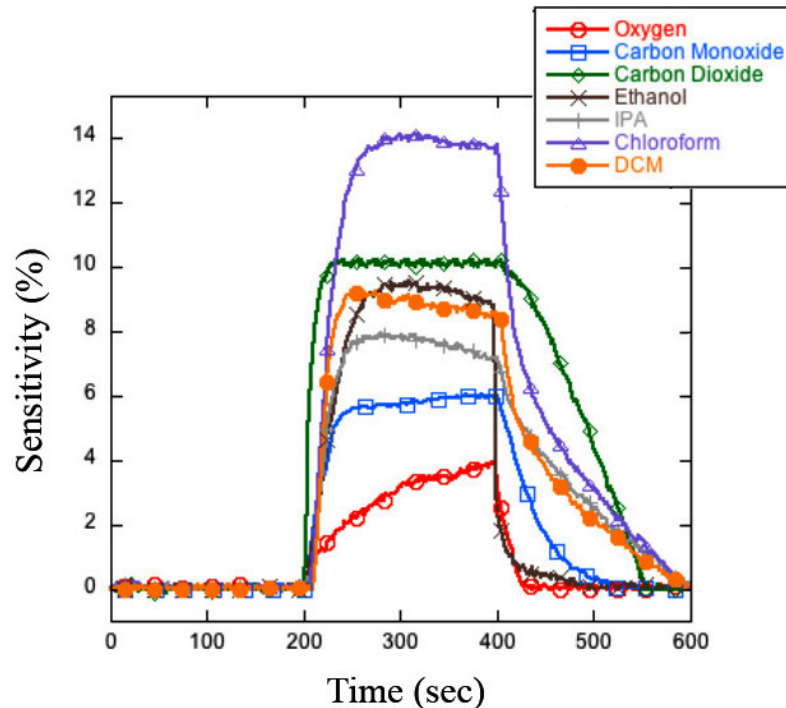


Figure 4.24 Sensitivity values of ZnO nanorod gas sensor for used target gases.

5. CONCLUSION

In this section, the discussion of sonochemically grown ZnO nanorod based gas sensor characterization and the gas sensing measurements are presented.

In this thesis, ZnO nanorods grown from Zinc nitrate and HMT solutions at room-ambient by the sonochemical method. ZnO nanorods were grown successfully on a glass substrate above ZnO seed layer within an hour. This is very short time compared to traditional growth techniques. Therefore, it can be inferred that sonochemical growth process reduces the growth time drastically. The glass was used as a very good insulator, durable and the most effective substrate.

ZnO nanorods were synthesized in the presence of gold (Au) IDE electrodes. IDE Au electrodes were deposited by conventional photolithography technique above chromium layer to prepare stable electrodes.

The surface morphology, crystal structure and elemental analysis of the grown nanorods' sample were observed by optical microscope, SEM, EDS and Raman Spectroscopy techniques. The results of the applied techniques indicate that ZnO nanorods were densely synthesized, and sonochemical technique can be utilized for the growth of crystalline ZnO nanorods. Gas sensor characteristics suggest that sonochemical growth method is a very good candidate for gas sensor applications.

The results indicated that the seed layer is required for crystalline and densely grown nanorod network. The trials showed that ZnO nanorods are lying on the surface of glass substrate without the seed layer.

The gas sensing measurements were carried out for two oxidizing gases, which are O₂ and CO₂ and five reducing gases, which are CO,

C₂H₅OH, C₃H₇OH, CHCl₃, CH₂Cl₂. The measurements are done to observe the change in resistance of the sensing layer at room temperature. The response time found to be significantly short in the ZnO nanorod gas sensor. However, desorption of gases takes relatively longer time. This is contributed to atoms of gas molecules cannot be completely desorbed by N₂ gas. It was also found that the sensor is the most sensitive to chloroform. Sensor's sensitivity to CO₂, ethanol, IPA, DCM gases is similar.

As a result, sonochemically grown ZnO nanorod gas sensor can be used for chemical gas sensor applications to detect many different gases.

For the future studies;

- ZnO nanorod gas sensor will be examined under unlike temperatures and concentrations of the gases.
- More gases can be measured such as CH₄, SO₂, NO, NO₂ and NH₃. Because these gases are the most common gases in the mines and sewer systems.
- Composite ZnO structures can be grown with another n-type material. So, the sensitivity of ZnO to these gases can be compared.
- The sensor can be made sensitive for one or two gases to be used in the specific locations.
- Grown conditions can be changed to synthesis different types of ZnO nanostructures then gas sensing properties of the grown nanostructures can be studied.
- Heating system can be added to the sensor in order to completely clean the target gases after the measurement.

REFERENCES

1. Picraux, S.T. *Properties at the nanoscale*. Nanotechnology 2013; Available from: <http://global.britannica.com/EBchecked/topic/962484/nanotechnology/236436/Properties-at-the-nanoscale>.
2. Initiative, N.N. *What It Is and How It Works*. Nanotechnology 101; Available from: <http://www.nano.gov/nanotech-101/what>.
3. WHO. *Air pollution*. 2014; Available from: http://www.who.int/topics/air_pollution/en/.
4. Agency, U.S.E.P. *An Introduction to Indoor Air Quality (IAQ)*. Indoor Air Quality (IAQ) 2013; Available from: <http://www.epa.gov/iaq/ia-intro.html>.
5. Agency, U.S.E.P. *Carbon Monoxide*. 2014; Available from: <http://www.epa.gov/iaq/co.html>.
6. Agency, U.S.E.P. *Carbon Dioxide*. 2014; Available from: <http://www.epa.gov/climatechange/ghgemissions/gases/co2.html>.
7. Agency, U.S.E.P. *Volatile Organic Compounds (VOCs)*. 2012; Available from: <http://www.epa.gov/iaq/voc.html>.
8. Seiyama, T., et al., *A New Detector for Gaseous Components Using Semiconductive Thin Films*. Analytical Chemistry, 1962. 34(11): p. 1502-1503.
9. Taguchi, N., *Gas detecting device*. 1972, Google Patents.
10. Park, J., *Nanostructured semiconducting metal oxides for use in gas sensors*, in *Institute for Superconducting and Electronic Materials*. 2010, University of Wollongong.
11. H., K. and H. A., *Interactions of excited dye molecules and oxygen*. Ber Dtsch Chem Ges., 1931. 64: p. 2677-2686.
12. Persaud, K. and G. Dodd, *Analysis of discrimination mechanisms in the mammalian olfactory system using a model nose*. Nature, 1982. 299(5881): p. 352-355.
13. Korotcenkov, G., *Chemical Sensors Comprehensive Sensor Technologies Volume:4 Solid State Devices*. Sensors Technology Series, ed. J. Watson. Vol. 4. 2011, New York: Momentum Press.
14. Ruzyllo, J., *Semiconductors in 21st Century – The First Decade*. 2011, Penn State University.

15. Das, R. and G. Roy, *The Basic Properties (Morphology & Conduction) of Metal Oxide Semiconductors for Gas Sensing Application*. Researcher, 2013. 5(3): p. 76-81.
16. Fine, G.F., et al., *Metal oxide semi-conductor gas sensors in environmental monitoring*. Sensors (Basel), 2010. 10(6): p. 5469-502.
17. Pokhrel, S., et al., *Investigations of conduction mechanism in Cr₂O₃ gas sensing thick films by ac impedance spectroscopy and work function changes measurements*. Sensors and Actuators B: Chemical, 2008. 133(1): p. 78-83.
18. Zeng, W., et al., *Facile synthesis of NiO nanowires and their gas sensing performance*. Transactions of Nonferrous Metals Society of China, 2012. 22, Supplement 1(0): p. s100-s104.
19. Liu, X., et al., *A survey on gas sensing technology*. Sensors (Basel), 2012. 12(7): p. 9635-65.
20. Kanazawa, E., et al., *Metal oxide semiconductor N₂O sensor for medical use*. Sensors and Actuators B-Chemical, 2001. 77(1-2): p. 72-77.
21. Choi, K.J. and H.W. Jang, *One-dimensional oxide nanostructures as gas-sensing materials: review and issues*. Sensors (Basel), 2010. 10(4): p. 4083-99.
22. Li, Q.H., et al., *Thin film transistors fabricated by in situ growth of SnO₂ nanobelts on Au/Pt electrodes*. Applied Physics Letters, 2004. 85(10): p. 1805.
23. Arshak, K. and I. Gaidan, *Development of a novel gas sensor based on oxide thick films*. Materials Science and Engineering B-Solid State Materials for Advanced Technology, 2005. 118(1-3): p. 44-49.
24. Xiaofeng, S., et al., *A highly sensitive ethanol sensor based on mesoporous ZnO–SnO₂ nanofibers*. Nanotechnology, 2009. 20(7): p. 075501.
25. Haeng Yu, J. and G. Man Choi, *Electrical and CO gas sensing properties of ZnO–SnO₂ composites*. Sensors and Actuators B: Chemical, 1998. 52(3): p. 251-256.
26. Zhu, C.L., et al., *Synthesis and enhanced ethanol sensing properties of α -Fe₂O₃/ZnO heteronanostructures*. Sensors and Actuators B: Chemical, 2009. 140(1): p. 185-189.
27. Yoon, D.H., J.H. Yu, and G.M. Choi, *CO gas sensing properties of ZnO–CuO composite*. Sensors and Actuators B: Chemical, 1998. 46(1): p. 15-23.

28. Hemmati, S., et al., *Nanostructured SnO₂-ZnO sensors: Highly sensitive and selective to ethanol*. Sensors and Actuators B: Chemical, 2011. 160(1): p. 1298-1303.
29. Mondal, B., et al., *ZnO-SnO₂ based composite type gas sensor for selective hydrogen sensing*. Sensors and Actuators B: Chemical, 2014. 194(0): p. 389-396.
30. Zhu, B.L., et al., *Improvement in gas sensitivity of ZnO thick film to volatile organic compounds (VOCs) by adding TiO₂*. Materials Letters, 2004. 58(5): p. 624-629.
31. Choopun, S., N. Hongsith, and E. Wongrat, *Metal-Oxide Nanowires for Gas Sensors*, in *Nanowires - Recent Advances*. 2012, InTech.
32. Kim, H., Y. Kwon, and Y. Choe, *Fabrication of nanostructured ZnO film as a hole-conducting layer of organic photovoltaic cell*. Nanoscale Research Letters, 2013. 8(1): p. 240.
33. Bano, N., *Fabrication and Characterization of ZnO Nanorods Based Intrinsic White Light Emitting Diodes (LEDs)*, in *Department of Science and Technology (ITN)*. 2011, Linköpings University. p. 68.
34. Mishra, V.N. and R.P. Agarwal, *Sensitivity, response and recovery time of SnO₂ based thick-film sensor array for H₂, CO, CH₄ and LPG*. Microelectronics Journal, 1998. 29(11): p. 861-874.
35. Wang, C.H., X.F. Chu, and M.W. Wu, *Detection of H₂S down to ppb levels at room temperature using sensors based on ZnO nanorods*. Sensors and Actuators B-Chemical, 2006. 113(1): p. 320-323.
36. Arafat, M.M., et al., *Gas sensors based on one dimensional nanostructured metal-oxides: a review*. Sensors (Basel), 2012. 12(6): p. 7207-58.
37. Liang, S., et al., *Synthesis of morphology-controlled ZnO microstructures via a microwave-assisted hydrothermal method and their gas-sensing property*. Ultrason Sonochem, 2014. 21(4): p. 1335-42.
38. Tharsika, T., et al., *Co-synthesis of ZnO/SnO₂ mixed nanowires via a single-step carbothermal reduction method*. Ceramics International, 2014. 40(3): p. 5039-5042.
39. Hou, X., F. Zhou, and W. Liu, *A facile low-cost synthesis of ZnO nanorods via a solid-state reaction at low temperature*. Materials Letters, 2006. 60(29-30): p. 3786-3788.
40. Heo, Y.W., et al., *Growth of ZnO thin films on c-plane Al₂O₃ by molecular beam epitaxy using ozone as an oxygen source*. Applied Surface Science, 2006. 252(20): p. 7442-7448.

41. Aultimut International, L. *Advances In RF Sputtering*. Available from: <http://www.aultimut.com/technologies-2/plasma-processes/%20advances-in-rf-sputtering/>.
42. Al-Hardan, N.H., et al., *ZnO thin films for VOC sensing applications*. *Vacuum*, 2010. 85(1): p. 101-106.
43. Ozcelik, B.K. and C. Ergun, *Synthesis of ZnO nanoparticles by an aerosol process*. *Ceramics International*, 2014. 40(5): p. 7107-7116.
44. Fang, Y., et al., *Detailed Study on Photoluminescence Property and Growth Mechanism of ZnO Nanowire Arrays Grown by Thermal Evaporation*. *The Journal of Physical Chemistry C*, 2010. 114(29): p. 12469-12476.
45. Barron, A.R. *Chemical Vapor Deposition*. Available from: <http://cnx.org/contents/9bbbe39c-a840-4461-882c-e31f8a0125e6@2@2>.
46. Chien, F.S.-S., et al., *Fast-response ozone sensor with ZnO nanorods grown by chemical vapor deposition*. *Sensors and Actuators B: Chemical*, 2010. 144(1): p. 120-125.
47. Han, Z., et al., *Controlled growth of well-aligned ZnO nanowire arrays using the improved hydrothermal method*. *Journal of Semiconductors*, 2013. 34(6): p. 063002.
48. Shafi, K.V.P.M., et al., *Sonochemical preparation of nanosized amorphous Fe-Ni alloys*. *Journal of Applied Physics*, 1997. 81(10): p. 6901-6905.
49. Gedanken, A., et al., *Using sonochemical methods for the preparation of mesoporous materials and for the deposition of catalysts into the mesopores*. (0947-6539 (Print)).
50. Nayak, A.P., et al. *Sonochemical Synthesis of Zinc Oxide Nanowire Arrays on Silicon and Glass Substrates*. in *The National Conference On Undergraduate Research (NCUR)*. 2010.
51. Anandan, S. and M. Ashokkumar, *Sonochemical Preparation of Monometallic, Bimetallic and Metal-Loaded Semiconductor Nanoparticles*, in *Theoretical and Experimental Sonochemistry Involving Inorganic Systems*, M. Ashokkumar, Editor. 2011, Springer Netherlands. p. 151-169.
52. Shimanovich, U., et al., *Proteinaceous microspheres for targeted RNA delivery prepared by an ultrasonic emulsification method*. *Journal of Materials Chemistry B*, 2013. 1(1): p. 82-90.
53. Eugene, O. and J. Soo-Hwan, *Sonochemical Method for Fabricating a High-performance ZnO Nanorod Sensor for CO Gas Detection*. *Journal of the Korean Physical Society*, 2011. 59(1): p. 8.

54. Zhu, H., D. Yang, and H. Zhang, *A simple and novel low-temperature hydrothermal synthesis of ZnO nanorods*. *Inorganic Materials*, 2006. 42(11): p. 1210-1214.
55. Patra, S.K., *A Novel Chemical Approach to Fabricate ZnO Nanostructures*, in *Department of Physics and Meteorology*. 2008, Indian Institute of Technology. p. 75.
56. Bradbury, S. *Scanning electron microscope (SEM)*. 2012; Art]. Available from: <http://global.britannica.com/EBchecked/media/110970/Scanning-electron-microscope>.
57. Wittke, J.H. *The Origin of Characteristic X-rays*. Art]. Available from: <http://www4.nau.edu/microanalysis/Microprobe/Xray-Characteristic.html>.
58. Williams, D.E., *Semiconducting oxides as gas-sensitive resistors*. *Sensors and Actuators B: Chemical*, 1999. 57(1-3): p. 1-16.
59. Kolmakov, A., et al., *Detection of CO and O₂ Using Tin Oxide Nanowire Sensors*. *Advanced Materials*, 2003. 15(12): p. 997-1000.
60. Gong, H., et al., *Nano-crystalline Cu-doped ZnO thin film gas sensor for CO*. *Sensors and Actuators B: Chemical*, 2006. 115(1): p. 247-251.
61. Kannan, P.K., R. Saraswathi, and J.B.B. Rayappan, *CO₂ gas sensing properties of DC reactive magnetron sputtered ZnO thin film*. *Ceramics International*, (0).
62. Van Hieu, N., et al., *Comparative study on CO₂ and CO sensing performance of LaOCl-coated ZnO nanowires*. *Journal of Hazardous Materials*, 2013. 244-245(0): p. 209-216.
63. Chou, S.M., et al., *ZnO : Al thin film gas sensor for detection of ethanol vapor*. *Sensors*, 2006. 6(10): p. 1420-1427.
64. Pawar, N.K., et al., *Nanostructured Fe₂O₃ Thick Film as an Ethanol Sensor*. *International Journal on Smart Sensing and Intelligent Systems*, 2012. 5(2): p. 441-457.
65. Streitwieser, A.j. and C. Heathcock, *Introduction to organic chemistry*. 1976, Newyork: Macmillan.
66. Bianchini, C., et al., *Selective oxidation of ethanol to acetic acid in highly efficient polymer electrolyte membrane-direct ethanol fuel cells*. *Electrochemistry Communications*, 2009. 11(5): p. 1077-1080.
67. Kulkarni, D. and I.E. Wachs, *Isopropanol oxidation by pure metal oxide catalysts: number of active surface sites and turnover frequencies*. *Applied Catalysis A: General*, 2002. 237(1-2): p. 121-137.

68. Cai, X., et al., *Isopropanol sensing properties of coral-like ZnO–CdO composites by flash preparation via self-sustained decomposition of metal–organic complexes*. *Sensors and Actuators B: Chemical*, 2014. 198: p. 402-410.
69. Perillo, P.M. and D.F. Rodríguez, *A room temperature chloroform sensor using TiO₂ nanotubes*. *Sensors and Actuators B: Chemical*, 2014. 193(0): p. 263-266.
70. Park, Y.H., et al., *Fabrication and its characteristics of metal-loaded TiO₂/SnO₂ thick-film gas sensor for detecting dichloromethane*. *Journal of Industrial and Engineering Chemistry*, 2008. 14(6): p. 818-823.
71. Lee, S.C., et al., *Novel SnO₂-based gas sensors promoted with metal oxides for the detection of dichloromethane*. *Sensors and Actuators B: Chemical*, 2009. 138(2): p. 446-452.
72. Wang, L., M. Sakurai, and H. Kameyama, *Catalytic oxidation of dichloromethane and toluene over platinum alumite catalyst*. *Journal of Hazardous Materials*, 2008. 154(1–3): p. 390-395.
73. Nayak, A.P., et al., *UV and Oxygen Sensing Properties and Space Charge Limited Transport of Sonochemically Grown ZnO Nanowires*. *Nanoscience and Nanotechnology Letters*, 2012. 4(10): p. 977-982.
74. He, C.X., et al., *Sonochemical Preparation of Hierarchical ZnO Hollow Spheres for Efficient Dye-Sensitized Solar Cells*. *Chemistry-a European Journal*, 2010. 16(29): p. 8757-8761.
75. Wang, N., et al., *Sono-assisted preparation of highly-efficient peroxidase-like Fe₃O₄ magnetic nanoparticles for catalytic removal of organic pollutants with H₂O₂*. *Ultrasonics Sonochemistry*, 2010. 17(3): p. 526-533.
76. Aurbach, D., et al., *Nanoparticles of SnO produced by sonochemistry as anode materials for rechargeable lithium batteries*. *Chemistry of Materials*, 2002. 14(10): p. 4155-4163.
77. Wang, Y.Q., et al., *Mesoporous titanium dioxide: sonochemical synthesis and application in dye-sensitized solar cells*. *Journal of Materials Chemistry*, 2001. 11(2): p. 521-526.
78. Mizukoshi, Y., et al., *Immobilization of noble metal nanoparticles on the surface of TiO₂ by the sonochemical method: Photocatalytic production of hydrogen from an aqueous solution of ethanol*. *Ultrasonics Sonochemistry*, 2007. 14(3): p. 387-392.

79. Oh, E., et al., *High-performance NO₂ gas sensor based on ZnO nanorod grown by ultrasonic irradiation*. Sensors and Actuators B-Chemical, 2009. 141(1): p. 239-243.
80. Ghaemi, M., et al., *Charge storage mechanism of sonochemically prepared MnO₂ as supercapacitor electrode: Effects of physisorbed water and proton conduction*. Electrochimica Acta, 2008. 53(14): p. 4607-4614.
81. Suslick, K.S., et al., *Characterization of sonochemically prepared proteinaceous microspheres*. Ultrasonics Sonochemistry, 1994. 1(1): p. S65-S68.
82. Wang, L., et al., *ZnO nanorod gas sensor for ethanol detection*. Sensors and Actuators B: Chemical, 2012. 162(1): p. 237-243.
83. Hsueh, T.J., et al., *ZnO nanowire-based CO sensors prepared on patterned ZnO : Ga/SiO₂/Si templates*. Sensors and Actuators B-Chemical, 2007. 125(2): p. 498-503.
84. Jiaqiang, X., et al., *Hydrothermal synthesis and gas sensing characters of ZnO nanorods*. Sensors and Actuators B: Chemical, 2006. 113(1): p. 526-531.
85. Erol, A., et al., *Humidity-sensing properties of a ZnO nanowire film as measured with a QCM*. Sensors and Actuators B-Chemical, 2011. 152(1): p. 115-120.
86. Van Quy, N., et al., *Gas sensing properties at room temperature of a quartz crystal microbalance coated with ZnO nanorods*. Sensors and Actuators B: Chemical, 2011. 153(1): p. 188-193.
87. Wan, Q., et al., *Fabrication and ethanol sensing characteristics of ZnO nanowire gas sensors*. Applied Physics Letters, 2004. 84(18): p. 3654-3656.
88. Xia, H., et al., *Development of film sensors based on ZnO nanoparticles for amine gas detection*. Applied Surface Science, 2011. 258(1): p. 254-259.
89. Peng, S., et al., *Application of Flower-Like ZnO Nanorods Gas Sensor Detecting Decomposition Products*. Journal of Nanomaterials, 2013. 2013: p. 7.
90. Wang, X.H., J. Zhang, and Z.Q. Zhu, *Ammonia sensing characteristics of ZnO nanowires studied by quartz crystal microbalance*. Applied Surface Science, 2006. 252(6): p. 2404-2411.
91. Joshi, R.K., et al., *Au Decorated Zinc Oxide Nanowires for CO Sensing*. Journal of Physical Chemistry C, 2009. 113(36): p. 16199-16202.

92. Lin, S.W., et al., *A selective room temperature formaldehyde gas sensor using TiO₂ nanotube arrays*. Sensors and Actuators B-Chemical, 2011. 156(2): p. 505-509.
93. Zhang, D., et al., *Detection of NO₂ down to ppb Levels Using Individual and Multiple In₂O₃ Nanowire Devices*. Nano Letters, 2004. 4(10): p. 1919-1924.
94. Sun, P., et al., *Hydrothermal synthesis of 3D urchin-like alpha-Fe₂O₃ nanostructure for gas sensor*. Sensors and Actuators B-Chemical, 2012. 173: p. 52-57.
95. Ryzhikov, A., M. Labeau, and A. Gaskov, *Al₂O₃(M = Pt, Ru) catalytic membranes for selective semiconductor gas sensors*. Sensors and Actuators B: Chemical, 2005. 109(1): p. 91-96.
96. Sharma, A., M. Tomar, and V. Gupta, *SnO₂ thin film sensor with enhanced response for NO₂ gas at lower temperatures*. Sensors and Actuators B-Chemical, 2011. 156(2): p. 743-752.
97. Kolmakov, A. and M. Moskovits, *Chemical sensing and catalysis by one-dimensional metal-oxide nanostructures*. Annual Review of Materials Research, 2004. 34(1): p. 151-180.
98. Chatterjee, A.P., P. Mitra, and A.K. Mukhopadhyay, *Chemically deposited zinc oxide thin film gas sensor*. Journal of Materials Science, 1999. 34(17): p. 4225-4231.
99. Wang, J.X., et al., *Hydrothermally grown oriented ZnO nanorod arrays for gas sensing applications*. Nanotechnology, 2006. 17(19): p. 4995.
100. Opel, M., *Spintronic oxides grown by laser-MBE*. Journal of Physics D-Applied Physics, 2012. 45(3): p. 033001.
101. [CC0], J. *Hexamine-3D-Balls*. 2011; Available from: <http://commons.wikimedia.org/wiki/File%3AHexamine-3D-balls.png>.
102. Coakley, M., *Growth and Optical Characterization of Zinc Oxide Nanowires for Anti-reflection Coatings for Solar Cells*, in *Physics*. 2011, Portland State University.
103. Fan, Z. and J.G. Lu, *Zinc oxide nanostructures: synthesis and properties*. (1533-4880 (Print)).

CURRICULUM VITAE



Name Surname: Enis Ekmel Tural

Place and Date of Birth: 20 July 1988/ Izmir, TURKEY

Address: 119 sok. No:30 D:3 Esenyalı Mah. Izmir, TURKEY

E-Mail: eetural88@gmail.com

B.Sc.: Environmental Engineering

Professional Experience and Rewards:

2012 to-date: Nanotechnology Master Program, Institute of Science/
Gediz University, Izmir/TURKEY.

2007 - 2011: Environmental Engineering, Faculty of Engineering/
Fatih University, Istanbul/TURKEY.

2010: Graduate Internship, Municipal Water Treatment Unit, IZSU,
Izmir/Turkey

2009: Graduate Internship, Provincial Directorate of Environment and
Urbanization, Izmir/Turkey

Conference Presentation on The Thesis:

Enis Ekmel Tural, Cebraıl Özbek, Salih Okur and Yavuz Bayam;
Sonochemically Grown ZnO Nanorods for CO Sensing; ISSTC
International Semiconductor Science & Technology Conference, January
13-15, 2014, Istanbul/TURKEY

Qualifications

Foreign languages: English: Very good speaking, writing, reading skills.

Computer skills: Excellent in Windows and Mac OS X; Microsoft Office (Word, Excel, Power Point); Apple iWork (Pages, Keynote, Numbers); Scientific Graphing and Data Analysis Softwares (Origin, Kaleida Graph, etc.); AutoCad.